②

NAVAL POSTGRADUATE SCHOOL
Monterey, California

THESIS

A METHOD OF TESTING TWO-DIMENSIONAL
AIRFOILS

BY
RICHARD KIRK JOYCE
March 1992

Thesis Advisor: R. M. Howard

92-19817

92 7 22 015

REPORT DOCUMENTATION PAGE

Form Approved
OMB No. 0704-0188

1a REPORT SECURITY CLASSIFICATION	1b. RESTRICTIVE MARKINGS
UNCLASSIFIED	

2a SECURITY CLASSIFICATION AUTHORITY	3. DISTRIBUTION/AVAILABILITY OF REPORT
2b DECLASSIFICATION/DOWNGRADING SCHEDULE	

4 PERFORMING ORGANIZATION REPORT NUMBER(S)	5. MONITORING ORGANIZATION REPORT NUMBER(S)

6a. NAME OF PERFORMING ORGANIZATION	6b. OFFICE SYMBOL (If applicable) 31	7a. NAME OF MONITORING ORGANIZATION
NAVAL POSTGRADUATE SCHOOL		NAVAL POSTGRADUATE SCHOOL

6c. ADDRESS (City, State, and ZIP Code)	7b. ADDRESS (City, State, and ZIP Code)
MONTEREY, CA 93943-5000	MONTEREY, CA 93943-5000

8a. NAME OF FUNDING/SPONSORING ORGANIZATION	8b. OFFICE SYMBOL (If applicable)	9. PROCUREMENT INSTRUMENT IDENTIFICATION NUMBER

8c. ADDRESS (City, State, and ZIP Code)	10. SOURCE OF FUNDING NUMBERS			
	PROGRAM ELEMENT NO.	PROJECT NO.	TASK NO.	WORK UNIT ACCESSION NO.

11. TITLE (Include Security Classification) A METHOD OF TESTING TWO-DIMENSIONAL AIRFOILS - UNCLASSIFIED

12 PERSONAL AUTHOR(S) LT RICHARD KIRK JOYCE, USN

13a. TYPE OF REPORT	13b. TIME COVERED	14. DATE OF REPORT (Year, Month, Day)	15 PAGE COUNT
MASTER'S THESIS	FROM _____ TO _____	MARCH 1992	69

16 SUPPLEMENTARY NOTATION THE VIEWS EXPRESSED IN THIS THESIS ARE THOSE OF THE AUTHOR AND DO NOT REFLECT THE OFFICIAL POLICY OR POSITION OF THE DEPARTMENT OF DEFENSE OR THE U.S. GOVERNMENT.

17	COSATI CODES		18 SUBJECT TERMS (Continue on reverse if necessary and identify by block number)
FIELD	GROUP	SUB-GROUP	TWO DIMENSIONAL AIRFOIL TESTING WITH STRAIN-GAGE BALANCES

19 ABSTRACT (Continue on reverse if necessary and identify by block number)

The Naval Postgraduate School Aeronautics and Astronautics Department conducts research and development for the Navy's Unmanned Air Vehicle program. NPS currently lacks the capability of testing two-dimensional airfoils to obtain lift, drag and pitching moment coefficients. This thesis consists of the design and calibration of a method of measuring these coefficients using strain gages, and the method of obtaining purely two-dimensional flow over the airfoil. During the calibration process, two amplifiers were tested in an attempt to minimize system drift and to ensure repeatability during successive runs. These desired characteristics were not achieved, however. The final phase was to be validation of the design by testing an NACA 0012 airfoil and comparing measured airfoil data with established reference data. This final phase was not completed due to structural failure of the airfoil.

20 DISTRIBUTION/AVAILABILITY OF ABSTRACT	21. ABSTRACT SECURITY CLASSIFICATION
☐ UNCLASSIFIED/UNLIMITED ☐ SAME AS RPT. ☐ DTIC USERS	UNCLASSIFIED

22a NAME OF RESPONSIBLE INDIVIDUAL	22b. TELEPHONE (Include Area Code)	22c OFFICE SYMBOL
R.M. HOWARD, PROFESSOR	408 646-2491	AA/HO

DD Form 1473, JUN 86

Previous editions are obsolete.

SECURITY CLASSIFICATION OF THIS PAGE

S/N 0102-LF-014-6603

Approved for public release; distribution is unlimited

A Method of Testing Two-Dimensional Airfoils

by

Richard Kirk Joyce
Lieutenant, U.S. Navy
B.S., Florida Institute of Technology, 1985

Submitted in partial fulfillment of the
requirements for the degree of

MASTER OF SCIENCE IN
AERONAUTICAL ENGINEERING

from the

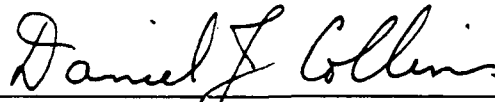NAVAL POSTGRADUATE SCHOOL

March 1992

Author: _____
Richard Kirk Joyce

Approved by: _____
Richard M. Howard, Advisor

Approved by: _____
Oscar Biblarz, Second Reader

_____
Daniel J. Collins, Chairman
Aeronautics and Astronautics

ii

ABSTRACT

The Naval Postgraduate School Aeronautics and Astronautics Department conducts research and development for the Navy's Unmanned Air Vehicle program. NPS currently lacks the capability of testing two-dimensional airfoils to obtain lift, drag and pitching moment coefficients. This thesis consists of the design and calibration of a method of measuring these coefficients using strain gages, and the method of obtaining purely two-dimensional flow over the airfoil. During the calibration process, two amplifiers were tested in an attempt to minimize system drift and to ensure repeatability during successive runs. These desired characteristics were not achieved, however. The final phase was to be validation of the design by testing an NACA 0012 airfoil and comparing measured airfoil data with established reference data. This final phase was not completed due to structural failure of the airfoil.

Accesion For		
NTIS CRA&I	☑	
DTIC TAB	☐	
Unannounced	☐	
Justification		
By		
Distribution /		
Availability Codes		
Dist	Avail and/or Special	
A-1		

TABLE OF CONTENTS

LIST OF TABLES

LIST OF FIGURES

I. INTRODUCTION

A. JUSTIFICATION

In June 1982, the Israelis attacked Syrian troops in the Bekaa Valley during the Israel-Lebanon conflict. The success of the attack can be attributed, at least in part, to the use of unmanned air vehicles (UAVs). The UAVs provided reconnaissance data on surface-to-air missile (SAM) sites enabling their destruction, battle damage assessment (BDA), and enemy troop movements. On 4 December 1983 two U.S. Navy aircraft were shot down, with one pilot killed and one crewman captured during a retaliatory strike on Syrian troops in Lebanon. Following these losses, the U.S. Navy realized the value of UAVs, and proceeded to procure a UAV system for the U.S. Navy and Marine Corps. In 1986, the Pioneer was selected to serve as the Navy's and Marine Corps UAV [Ref. 1].

Since the procurement of the Pioneer, the Naval Postgraduate School (NPS) Aeronautics and Astronautics Department has established a UAV Research Program with a half-scale model of the Pioneer. The purpose of the NPS-UAV program is to provide research testbeds for inflight research projects and a test and evaluation capability to investigate methods of improving and/or validating the performance of the Pioneer, as well as other current or future UAVs.

NPS, however, currently lacks the capability of performing two-dimensional low Reynolds number airfoil testing. Development of a method to perform such testing would increase the scope of the NPS UAV research, development, test and evaluation program.

B. THESIS SCOPE

The scope of this thesis is to design, construct, calibrate, and validate a method to obtain lift, drag, and pitching moment coefficients of a two-dimensional airfoil at low Reynolds numbers.

The design phase consists of developing a method to obtain two-dimensional flow over the airfoil, as well as design of the strain gage balance used to obtain lift, drag, and pitching moment measurements. Calibration of the strain gage balance is conducted to determine the influence matrix of the balance system. To validate the developed method, lift, drag and pitching moment coefficients of a two-dimensional, NACA-0012 airfoil is determined experimentally and compared to existing reference data.

II. BACKGROUND

In order to evaluate airfoil designs, an accurate method of determining two-dimensional lift, drag, and pitching moment coefficients is required. Simulating two-dimensional flow in the confined environment of a wind tunnel has always posed a challenge.

Most of the currently used NACA airfoil section data were measured in wind tunnels during the 1930's and 1940's. The earliest test models were wings with various wing-tip fairings and end plates. Forces and moment data were obtained using a six-component balance and corrections for aspect ratio were applied. Beginning in 1941, tests conducted in the NASA Langley two-dimensional low-turbulence wind tunnels used models of two-foot chord spanning the three-foot wide test section. Measurement of the pressure distributions on the ceiling and floor of the test section provided airfoil lift data, and wake surveys measuring momentum loss provided drag data.

The primary concern in airfoil testing is three dimensional flow, which exists at the airfoil-sidewall junction due to boundary-layer interaction, shown in Figure 2.1. There are conflicting conclusions as to the actual effects of the airfoil-sidewall boundary-layer interaction on lift, drag, and pitching moment data. According to Treaster, drag data, with traditional corrections applied, for an airfoil that spans a rectangular test section can vary by as much as an order of magnitude from established reference data [Ref. 2]. Mueller [Refs. 3,4] evaluated the effects of the airfoil-sidewall boundary layer interaction using one-piece and three-piece airfoil models, shown in Figures 2.2 and 2.3 respectively, and found the minimum drag coefficient of the three-piece airfoil to be about 16 percent lower than that for the one-piece airfoil. The effects on lift and pitching moment data, according to both Treaster and Rogers [Ref. 5], are negligible.

3
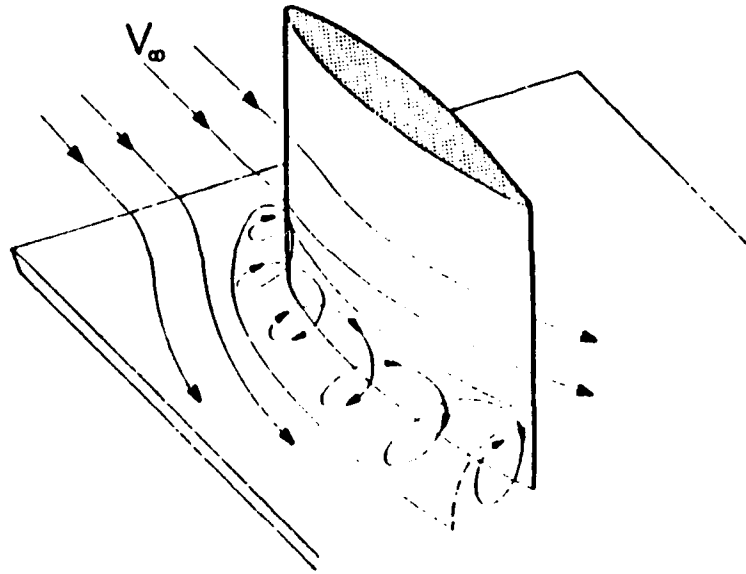
Figure 2.1: Airfoil-sidewall Boundary Layer Interaction

The measured lift and pitching moment data from this study were in agreement with established reference data. For an airfoil mounted between the test section sidewalls, Mokry [Ref. 6] and van der Bliek [Ref. 7] concluded that the three-dimensional flow at the airfoil-sidewall junction changes the lift distribution for the portion of the airfoil within the corner vortex. At high angles of attack, flow separation at the junction caused a span-wise variation of pitching moment.

According to Jacobs [Ref. 8] and Gorlin [Ref. 9], the effects of the airfoil-sidewall boundary layer interaction can be negated if dummy airfoils extend, from the sidewall, the thickness of the disturbed region. There are also conflicting theories as to the extent of the disturbed region. Mueller has shown the disturbed region, at low chord Reynolds numbers (i.e., R_c, 100,000), to be as large as 10 percent (of the 412 mm span) for a two-dimensional FX 63-137 airfoil section spanning the sidewalls of a test section. This disturbed region will decrease in size and effect as Reynolds number increases.

4
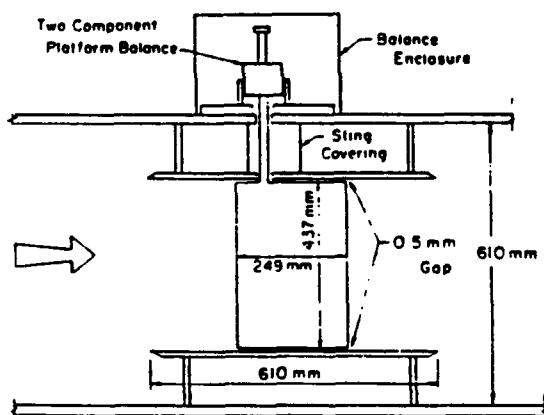
Figure 2.2: One-Piece Airfoil   Figure 2.3: Three-Piece Airfoil
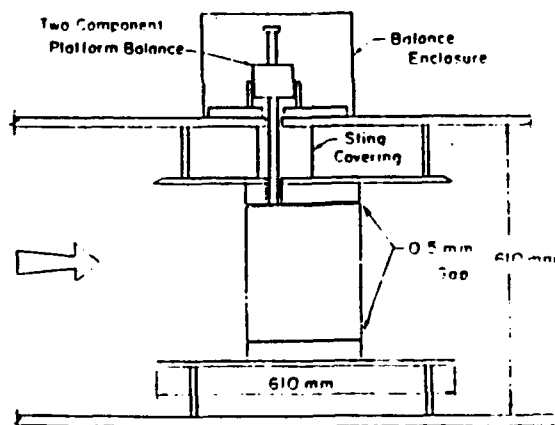
Wooltuft tests, conducted by van der Bliek on a two-dimensional airfoil spanning the test section sidewalls, indicated the disturbed region extended to a line 45 degrees from the airfoil leading edge and sidewall junction.

As a result of selecting the three-piece airfoil design, chordwise gaps between the outer and center airfoil sections exist. The comparison of three-piece and one-piece airfoil data by Mueller is inconclusive. The lift coefficient differed slightly but inconsistently, and the minimum drag coefficient, measured for the two models, is overshadowed by the uncertainty in the measurements. Experiments by Kuppa [Ref. 10] and Marchman [Ref. 11], using a Wortmann FX63-137 airfoil with gaps between the airfoil and end plates, have shown that significant flow exists through any size gap, even as small as 0.1 mm. The minimum drag coefficient was shown to have the highest value for the case of the sealed gap and to decrease as gap size increased in the Reynolds number range from 100,000 to 300,000. The zero-lift angle of attack matched

established reference data when the gap was sealed, but increased from -11 degrees to -6 degrees with a 0.1 mm gap. The value C_{L_α} was also shown to decrease when a gap existed. Therefore, it was concluded that even flow through a small gap could represent a substantial portion of the airfoil's lift at low Reynolds numbers, resulting from early upper-surface separation on the airfoil due to gap flow. Although an airfoil with an end plate gap eliminates the necessity of correcting for plate drag, the other errors which are introduced may be quite large.

With the assumption that the effects of chordwise gaps within a three-piece airfoil and at an airfoil-end plate junction are similar, it was concluded the gaps must be sealed to obtain accurate aerodynamic data at low Reynolds numbers. Perry [Ref. 12] used petroleum jelly to seal the gaps but found that at an angle of attack greater than 8 degrees, he was unable to maintain the seal. Kuppa also concluded petroleum jelly was inadequate and conducted zero gap tests by sealing the gap with oil-soaked foam rubber weather stripping. Kuppa's results are in agreement with established reference data.

Based on the previous experiments discussed, the following design was deemed optimum for our two-dimensional airfoil testing. A three-piece airfoil is used with the outer airfoil sections attached to the vertical support structure, and the center airfoil section "floating" between them. Chordwise gaps exist between the outer and center airfoil sections to preclude contact. These gaps were sealed in a manner to prevent airflow through the gap, thus altering measured lift and drag data, and to prevent transmission of a force or moment across the gap. The outer airfoil sections extend from the vertical support structure into the test section, a distance equal to the chord. The region of disturbed airflow due to the airfoil-sidewall boundary layer interaction, taken to extend to a line 45 degrees from the airfoil leading edge-sidewall junction, only effects the flow on the outer airfoil sections. As a result, purely two-dimensional

6

flow exists over the center airfoil section which then can be used to obtain measured two-dimensional lift, drag, and pitching moment data, with the recognition that no separated flow is truly two-dimensional.

III. EXPERIMENTAL EQUIPMENT

The major items required during this investigation include the wind tunnel, three-piece airfoil, vertical support structure, strain-gage balance shafts, calibration bar, and the data acquisition system. This chapter describes the specifications, setup, and design of the equipment used.

A. WIND TUNNEL

The Naval Postgraduate School low speed horizontal wind tunnel was employed for this investigation. The tunnel, of wood construction, measuring 64 feet long and 25.5 feet wide, is shown in Figure 3.1.

The power section consists of a 100 horsepower electric motor, driving a three-bladed variable pitch fan. Eight stator blades, downstream of the fan, straighten the flow prior to one of the two diffuser sections, located on either side of the fan. The settling chamber, containing two fine wire anti-turbulence screens mounted six inches apart, and the contraction cone, of 10:1 ratio, tend to produce a more uniform distribution of velocity and decrease turbulent fluctuations in the test section.

The rectangular test section measuring 32 inches high, 45 inches wide, and 4 feet in length, with a reflection plane mounted 4 inches above the floor, has a cross-sectional area of 8.75 ft^2. The walls of the test section are slightly divergent to counteract the contraction resulting from boundary-layer growth. The corner lighting is provided within the corner fillets to illuminate the test section and reduce the effects of boundary layer interaction at the wall junctions. Downstream, breather slots allow air to flow into the circuit to make up for leakage losses and to maintain atmospheric pressure in the test section.
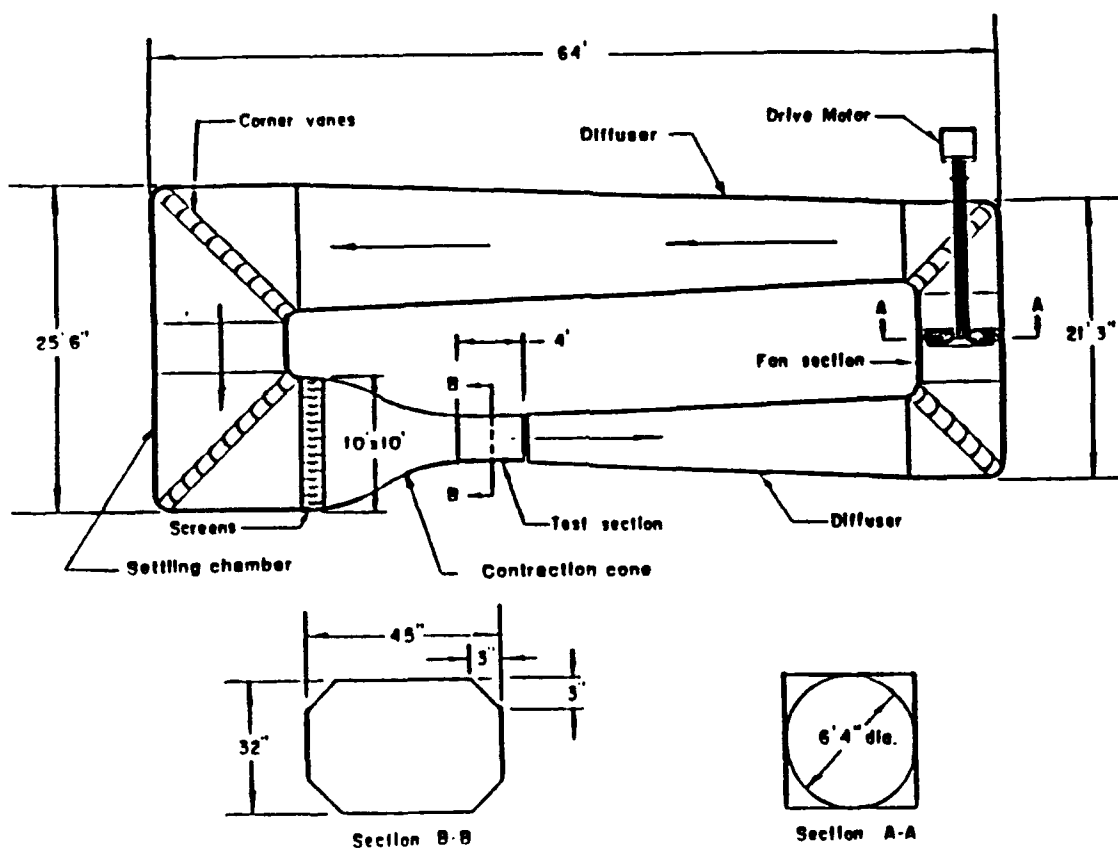
8

Figure 3.1: NPS Low Speed Wind Tunnel

Two sets of four static pressure ports are used to determine a test section velocity. One set is located in the settling chamber, downstream of the turbulence screens, and the other set is located in the contraction cone upstream of the test section [Ref. 13]. The wind tunnel test section calibration procedure and results are discussed in Chapter IV.

B. THREE-PIECE AIRFOIL

The wooden three-piece NACA 0012 airfoil spans 34.28 inches, excluding chordwise gaps, with an eight-inch chord. The three-piece airfoil is shown in Figure 3.2, and design drawings are contained in Appendix A.

The outer airfoil sections, each of eight-inch span, are mounted horizontally to rotatable inserts contained within the vertical supports shown in Figure 3.3. The center airfoil section, spanning 18.28 inches, is supported from each end, between the outer airfoil sections, by the strain-gage balance shafts. Spanwise cutouts through the outer airfoil sections at the quarter-chord point, measuring 0.7 x 1.2 inches, house the strain-gage balance shafts. The cutouts provide an end clearance of 0.065 inches for the calculated shaft deflection of 0.035 inches during application of a normal force of 113.0 lbf. The determination and discussion of these values were determined and are discussed in Section D of this chapter.

Chordwise gaps exist between the outer airfoil sections and the center airfoil section. Adjustment of these gaps are accomplished and fixed through the use of shims and an end plate on the outboard sides of the rotatable inserts. Chordwise gaps must exist to preclude the friction, due to outer airfoil and center airfoil section contact, from altering the measured forces and moment of the center airfoil section. The chordwise gaps, each of approximately 0.045 inches, were sealed using thin sheets of latex rubber due to its inability to transmit a force or moment across the gaps.

10
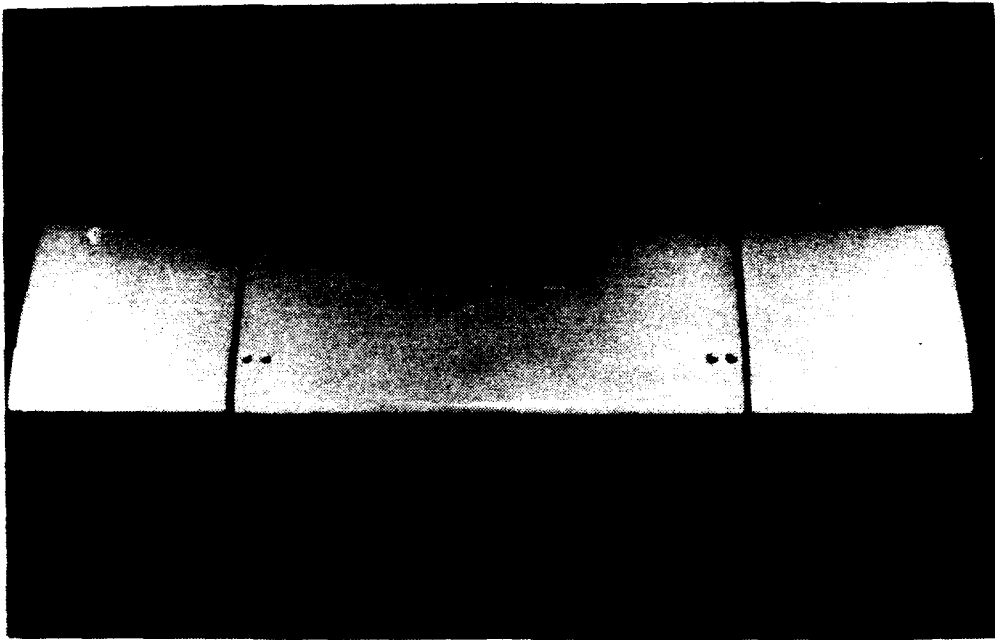
Figure 3.2: Three-Piece Airfoil
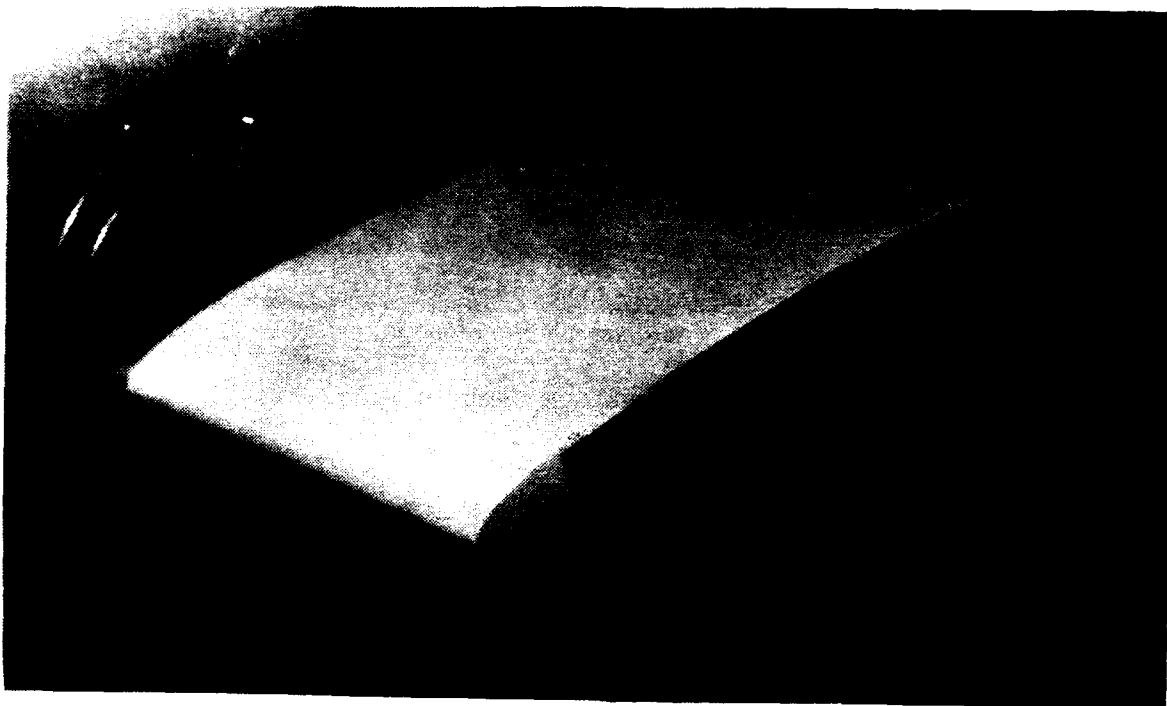
Figure 3.3: Outer Airfoil Section

C. VERTICAL SUPPORT STRUCTURE

The support structure, used for previous experiments at NPS, was modified for this application. It consists of two eight-inch wide aluminum plates which extend vertically from the reflection plane to the top wall of the test section. The three-piece airfoil spans horizontally between the supports with the outer airfoil sections and strain-gage balance shafts being mounted to rotatable inserts within the supports. Figure 3.4 shows the setup of the vertical support structure and three-piece airfoil.

The rotatable inserts provide the capability of manually adjusting and locking the three-piece airfoil at an angle of attack (AOA) in the range from +35 to -15 degrees. Due to the method of strain-gage balance shaft attachment [see Appendix A], as AOA is varied, the strain-gage balance shafts also rotate. As a result, the forces measured by the strain-gage balance shafts are forces which are normal and axial to the airfoil chord rather than to the free stream. Calibration curves, discussed in Chapter V, account for the force relationship with AOA.
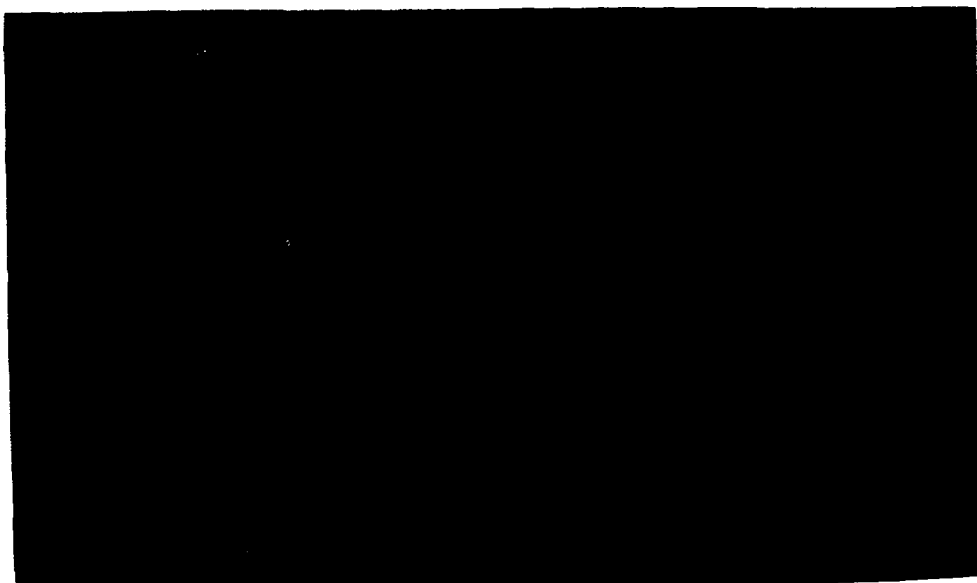
Figure 3.4: Vertical Support Structure and Three-Piece Airfoil Assembly

D. STRAIN-GAGE BALANCE SHAFTS

Since the outer airfoil sections contain cutouts for the strain-gage balance shafts, their design had a dimensional constraint due to the quarter-chord thickness of the airfoil less the shaft end deflection, clearance, gap, and airfoil material thickness required to maintain structural integrity. Design iterations were performed using shafts of various cross sections and combinations, optimizing shaft dimensions, end deflection, and surface strain used for measurements. Performance during a "worst-case" loading scenario was also investigated to preclude failure of the structure.

With airfoil values of lift coefficient (C_L), drag coefficient (C_D), pitching moment coefficient (C_M), and area (S) of:

$$C_L = 3.00$$

$$C_D = 0.08$$

$$C_M = -0.30$$

$$S = 1.014 \, ft^2$$

and chord Reynolds number (R_C), airfoil chord (C), density (ρ), and viscosity (μ) as follows.

$$R_C = 750,000$$

$$C = 0.667 ft$$

$$\rho = 2.3769x10^{-3} slug/ft^3$$

$$\mu = 3.7373x10^{-7} slug/ft \cdot s$$

Using the relationship of Equation 3.1 [Ref. 14]

$$R_c = \frac{\rho V c}{\mu} \tag{3.1}$$

the desired test section velocity (V) was calculated as 176.9 ft/s.

Design airfoil lift (L), drag (D), and pitching moment (M) defined by Equations 3.2, 3.3, and 3.4, respectively [Ref. 14]

$$L = \frac{1}{2}\rho v^2 S C_L \qquad (3.2)$$

$$D = \frac{1}{2}\rho v^2 S C_D \qquad (3.3)$$

$$M = \frac{1}{2}\rho v^2 S c C_M \qquad (3.4)$$

were calculated as follows.

$$L = 113.0 \; lbf$$

$$D = 3.0 \; lbf$$

$$M = 7.5 \; ft \cdot lbf$$

As previously discussed in Section C of this chapter, the values labeled lift and drag will only correspond to the actual forces measured by the strain-gage balance shafts at zero AOA. Otherwise, the strain-gage balance shafts will measure normal and axial components.

Iterations were performed using various shaft dimensions, cross sections and combinations of cross sections. The goal was to optimize the design considering shaft dimensions, end deflection, and surface strains. The optimum strain-gage balance shaft design is shown in Figure 3.5. Other design details are shown in Appendix A.

Moment of inertia (I) of a rectangular cross section is defined by Equation 3.5 [Ref. 18]. Deflection for a beam fixed at one end and free, but guided, at the other is defined by Equation 3.6. Equation 3.6 can be reduced to provide the free end deflection in the form of Equation 3.7 [Ref. 15]. Strain-gage balance shaft section properties are listed in Table 3.1.
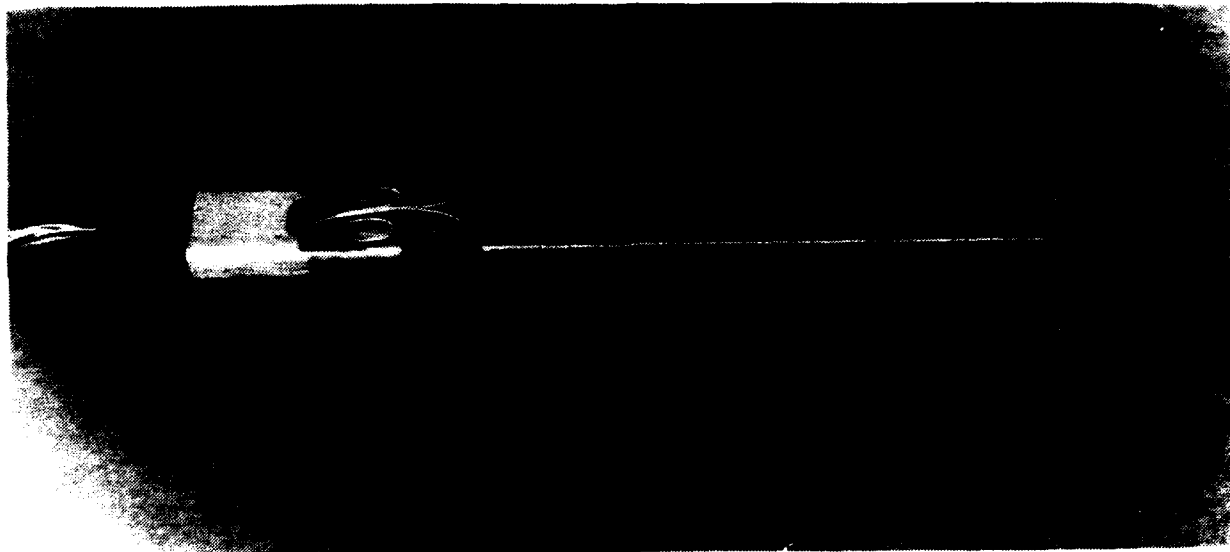
$$I = \frac{bh^3}{12} \qquad (3.5)$$

15

Figure 3.5: Strain-Gage Balance Shaft
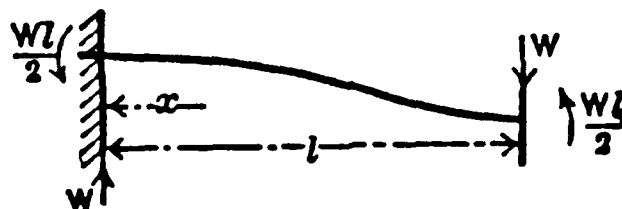
Figure 3.6: Beam Deflection, Fixed-Free and Guided

$$y = \frac{Wx^2}{12EI}(3l - 2x) \tag{3.6}$$

$$y = \frac{Wl^3}{12EI} \tag{3.7}$$

where W is the load applied at the free end, l is the beam length, and x is the distance from the fixed end as shown in Figure 3.6.

Strain-gages were mounted to the strain-gage balance shafts, at locations shown in Figure 3.7, using recommended procedures [Refs. 16, 17, and 18]. The strain-gages, Micro-Measurements Type CEA-13-250 UN-350, have a resistance (R) of 350.0 Ω $\pm$ 0.3% and a gage factor (F) of 2.12 $\pm$ 0.5% at 75° F. Using the relationship of Equation 3.8 [Ref. 19]

$$F = \frac{\Delta R/R}{\epsilon}$$ (3.8)

and the specifications of the data acquisition equipment, to be discussed in Section F of this chapter, the "target" strain value (ϵ) was determined to be 1.0 x 10^{-3} in/in. This value was determined to provide acceptable accuracy considering system drift and other "noise". This value could not be obtained for the axial force measurement. This fact is a result of the axial force being two orders of magnitude less than the normal force and the necessity to design the strain-gage balance shafts to preclude deformation and failure. Strain predictions were made using the relationships of Equations 3.9 and 3.10 [Ref. 20], resulting in Equation 3.11, where y is the distance from the neutral axis, and ρ is the radius of curvature.

$$\epsilon = \frac{-y}{\rho}$$ (3.9)

$$\frac{1}{\rho} = \frac{\mu}{EI}$$ (3.10)

$$\epsilon = \frac{-yM}{EI}$$ (3.11)

17
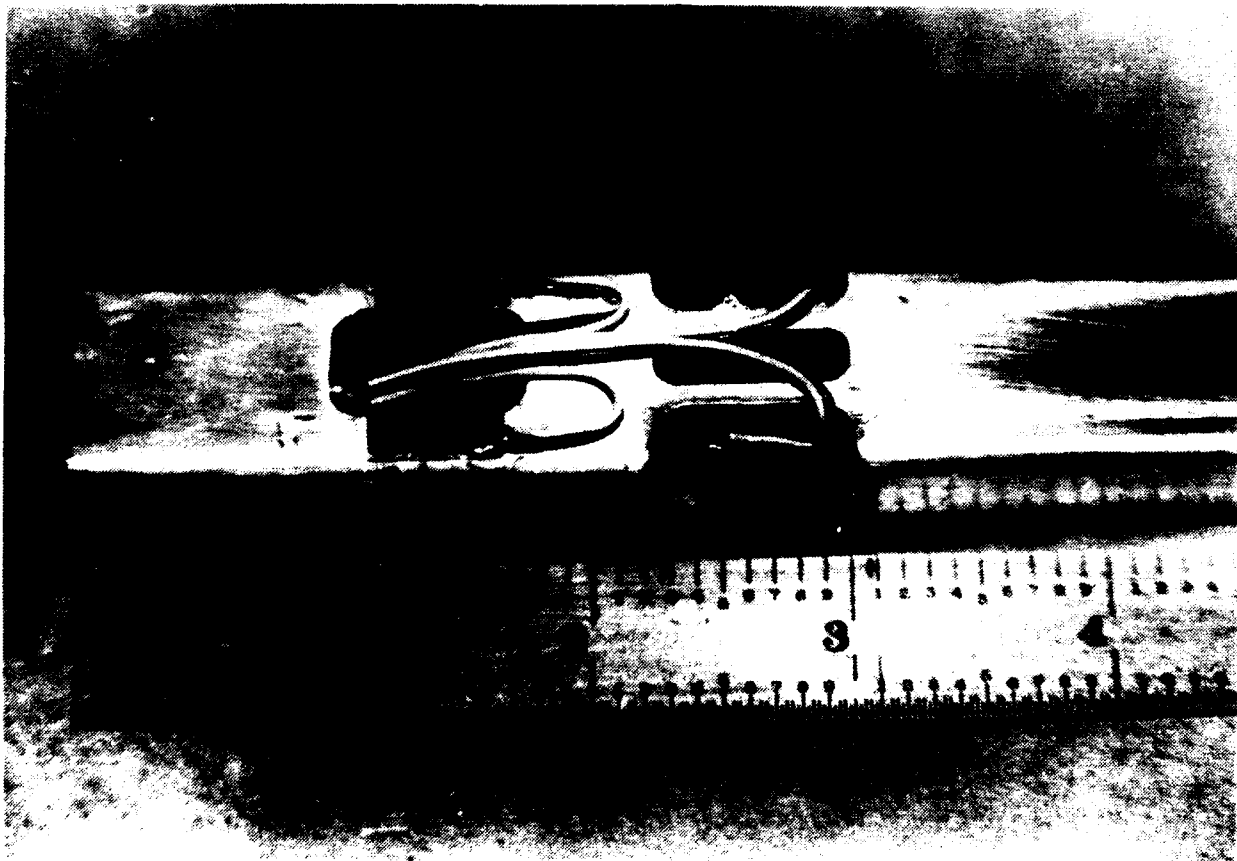
Figure 3.7: Strain-Gage Mounting Locations

18

The predicted surface strains at gage locations are listed in Table 3.1.

TABLE 3.1: STRAIN-GAGE BALANCE SHAFT SECTION PROPERTIES

	Section A-A	Section B-B	Section C-C
Normal Force I (in^4)	5.208 x 10^{-3}	2.083 x 10^{-3}	1.042 x 10^{-2}
Axial Force I (in^4)	3.646 x 10^{-2}	3.146 x 10^{-3}	
Strain gage location (in/in)	1.100 x 10^{-3}	4.300 x 10^{-5}	

The wheatstone bridge output voltages (E_o) are a function of gage factor (F), surface strain (ϵ), and excitation voltage (E). These values and relationships are:

$$F = 2.12$$

$$\epsilon_N = 1.1 \; x \; 10^{-3} \; in/in$$

$$\epsilon_A = 4.3 \; x \; 10^{-5} \; in/in$$

$$E = 5.00 Vdc$$

$$F = \frac{\frac{\Delta R}{R}}{\epsilon} \tag{3.12}$$

$$E_o = \frac{E}{4} \left(\frac{\Delta R_A}{R_A} - \frac{\Delta R_B}{R_B} + \frac{\Delta R_C}{R_C} - \frac{\Delta R_D}{R_D} \right) \tag{3.13}$$

R_A, R_B, R_C, and R_D form the legs of the wheatstone bridge in a clockwise fashion beginning at the upper left leg. E is applied across pins A and D with E_o measured across pins B and C as shown in Figures 3.8, 3.9, and 3.10.

19

Figure 3.8: Normal Component Wheatstone Bridge
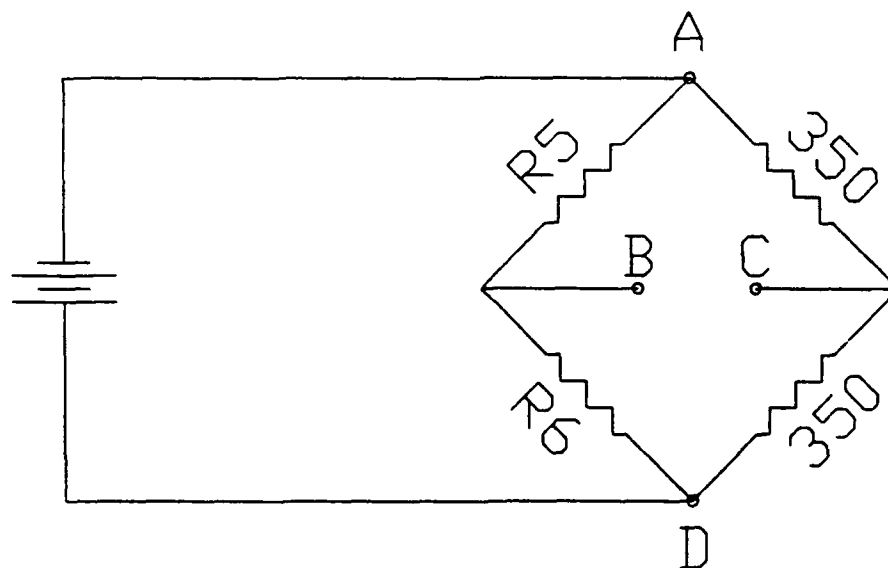
Figure 3.9: Axial Component Wheatstone Bridge
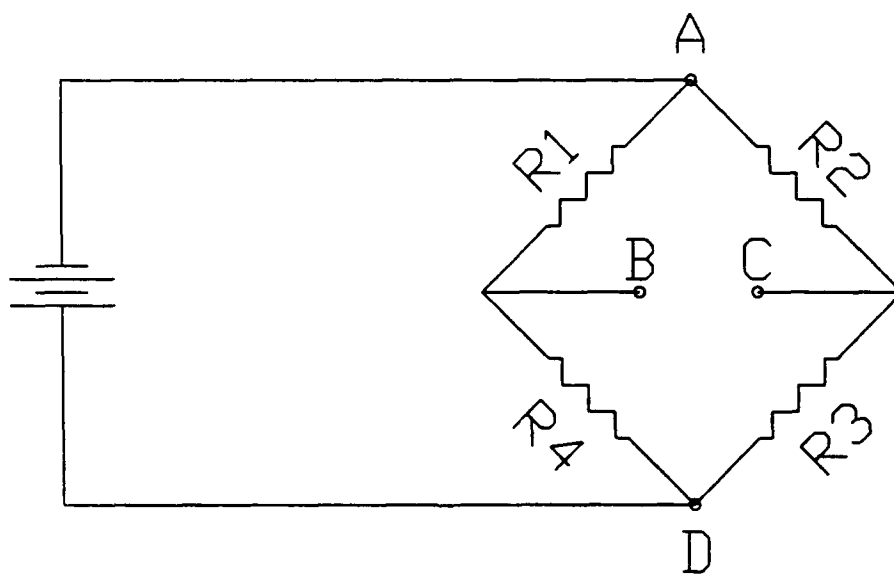
Figure 3.10: Pitching Moment Wheatstone Bridge

The wheatstone bridge output voltages for the normal and axial directions, respectively, were determined to be

$$(E_o)_N = 11.66 \, mVdc$$

$$(E_o)_A = 0.23 \, mVdc$$

After amplification at a gain of 1000, the voltages (at design loads) should be

Normal voltage output : $= 11.66 \, Vdc$

Axial voltage output : $= 0.23 \, Vdc$
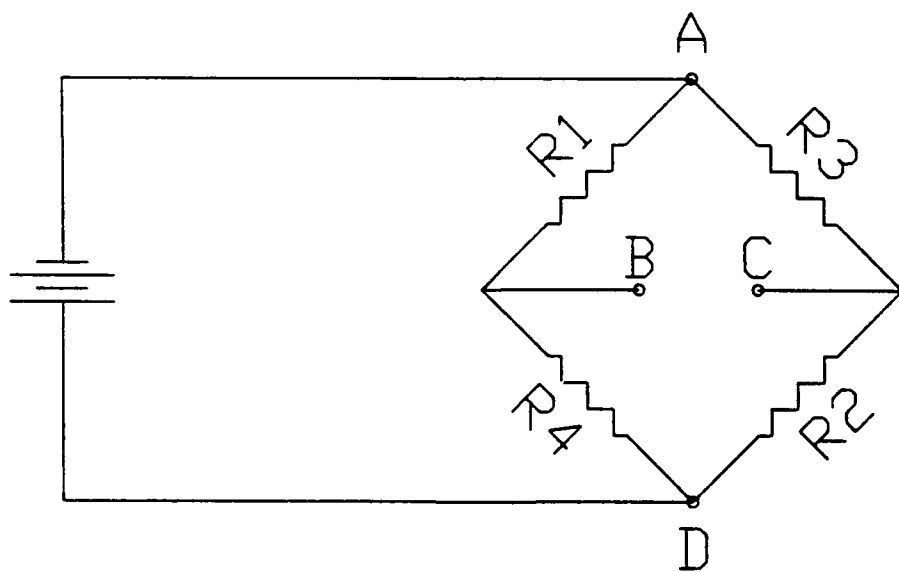
The strain-gage balance shaft end defections were determined using superposition of the deflections of all cross sections and were calculated to be 0.035 inches and 0.00036 inches for the normal and axial directions, respectively. The 1.2-inch-wide cutouts, through the quarter-chord of the outer airfoil sections will provide adequate clearance to preclude airfoil-shaft contact.

The strain-gage balance shafts will fit into inserts at the quarter-chord of the center airfoil section, and through-bolts prevented lateral movement or twisting. The outer ends were fitted into inserts within the rotatable inserts of the vertical support structure. A plate mounted on the outboard side of the rotatable insert prevented horizontal movement perpendicular to the flow and provide adjustment of the chordwise gaps. Set screws, within the rotatable inserts, prevented other lateral movement and twisting. Details are shown in Figure 3.11 and Appendix A.

E. CALIBRATION BAR

The calibration bar was constructed from 1.0 inch x 2.0 inch aluminum bar stock to reduce flexure and twisting during application of loads. Designed to replace the center airfoil section during the strain-gage balance shaft calibration process, its length is 18.28 inches and the inserts, within the ends of the calibration bar for the strain-gage

Figure 3.11: Rotatable Insert Mounting Assembly

balance shafts, are identical to those within the center airfoil section. At the center of the span is a threaded hole to allow attachment of an eye bolt used to apply the loads to the calibration bar during the strain-gage balance shaft calibration process discussed in Chapter IV. The calibration bar is shown in Figure 3.12 and design details can be found in Appendix A.

F. DATA ACQUISITION SYSTEM

The Data Acquisition System consists of a signal conditioner, relay multiplexer, amplifier, digital multimeter, and a microcomputer. The signal flow is shown in Figure 3.13.

1. Signal Conditioner

The 10-channel conditioner was used to provide and adjust the excitation voltages of the wheatstone bridges and to provide a zero and span adjustment of each wheatstone bridge output voltage via potentiometers located on the front panel. This procedure is discussed in Chapter IV.

The strain-gages were connected as previously shown in Figures 3.8, 3.9 and 3.10 to complete the circuitry for the wheatstone bridges. The cannon-plug pins are denoted by A, B, C, and D. The excitation voltages are applied across pins A and D, and the output voltages are measured between pins B and C. The cannon plugs, wired with the wheatstone bridges, are then connected to the rear of the signal conditioner.

2. Relay Multiplexer

A Hewlett-Packard PC Instruments Model 61011A Relay Multiplexer was used to sequentially route each channel's output voltage to the amplifier. The input and output connections are made via a terminal block on the front panel. The micro-computer, discussed later, controls the switching via the PC Instruments software.
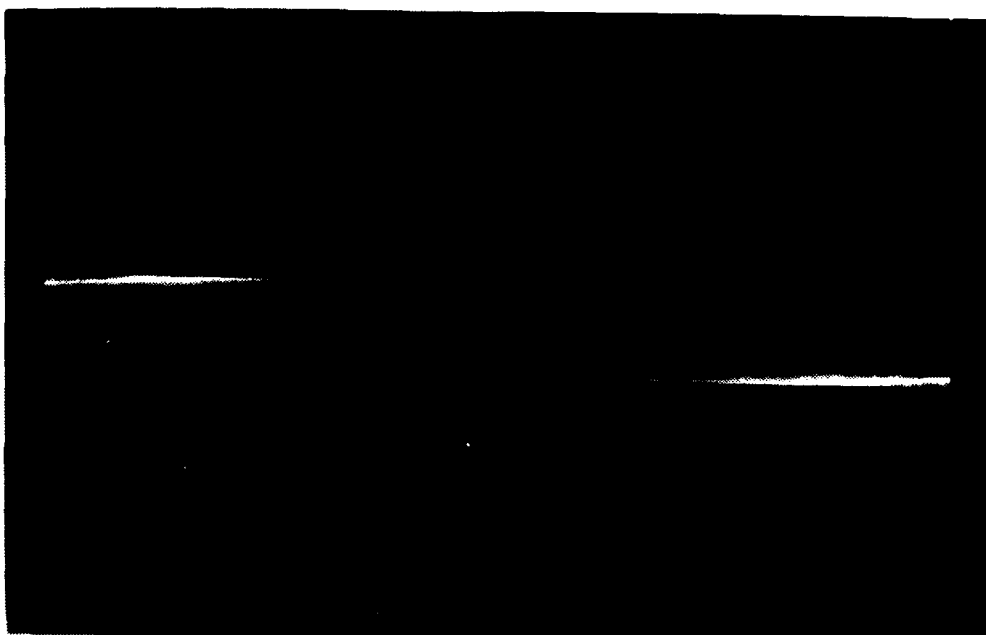
Figure 3.12: Calibration Bar
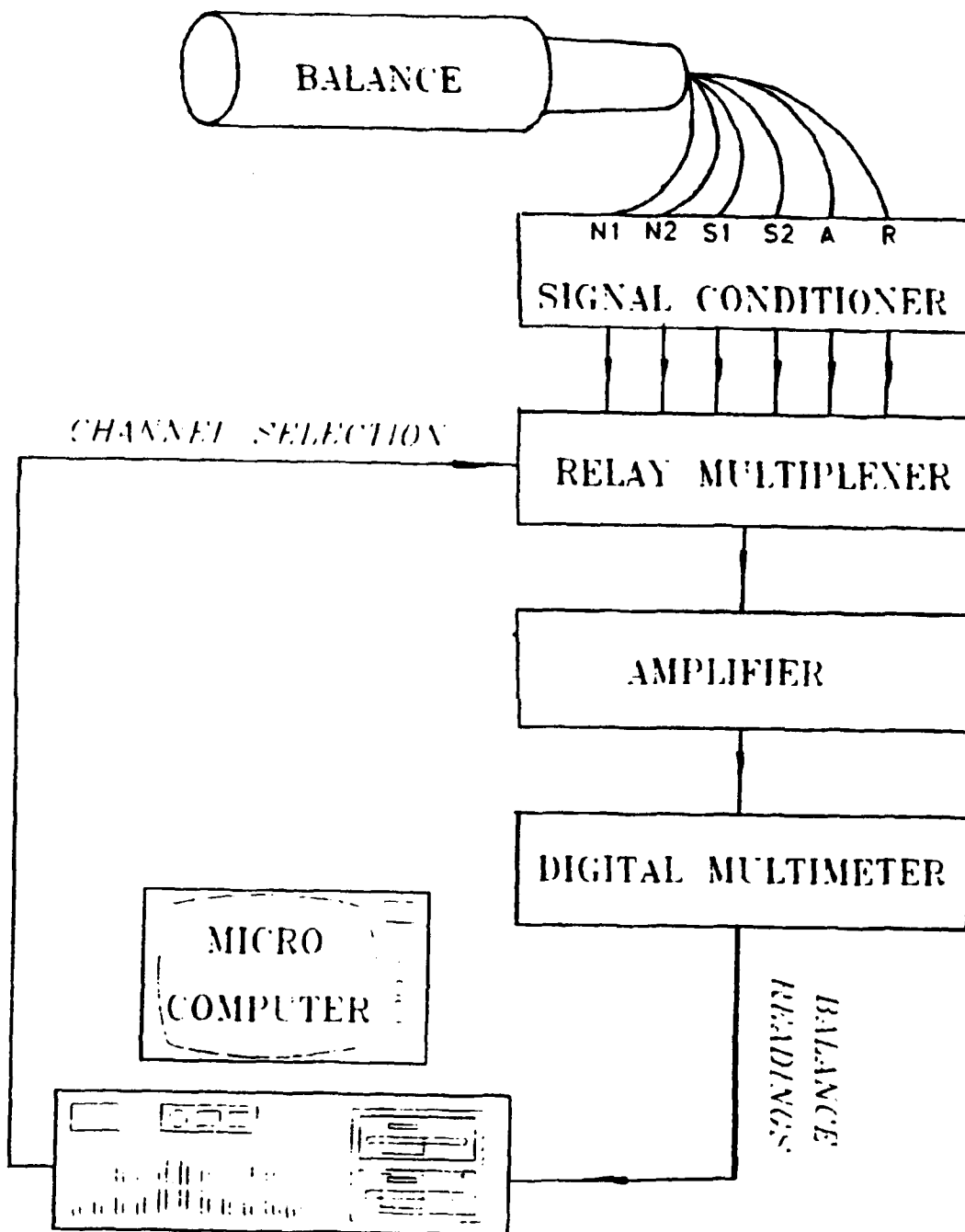
Figure 3.13: Data Acquisition System Signal Flow

3. Amplifier

The Pacific Instruments Model 8255 Amplifier was used to amplify the sequentially routed wheatstone bridge output voltages prior to measurement to improve resolution. The amplifier, used at a gain of 1000, has a accuracy of ± 0.1% and stability of ± 0.01%. The front panel contains the necessary adjustments to zero and to calibrate the amplifier. This procedure is discussed in Chapter IV. Input and output connections are made at the rear of the unit.

4. Digital Multimeter

A Hewlett-Packard PC Instruments Model 61013A Digital Multimeter (DMM) was used to measure the amplified wheatstone bridge output voltages. The measurements are performed, controlled and recorded by the microcomputer. Measurements were taken at a rate of 2.5 readings per second with resolution of at least 0.01 mVdc. The amplifier outputs are connected to the front panel of the DMM.

5. Microcomputer

An IBM-AT Microcomputer was used to control the functions of the DMM and relay multiplexer and to display the amplified wheatstone bridge output voltages. A soft front panel program entitled *PANELS* provided a $4\frac{1}{2}$ digit readout of the DMM output and allowed the selection of relay multiplexer channels via a cursor. The microcomputer was connected via an HP Interface Card and ribbon-cable bus to the rear of the HP PC Instruments.

IV. EXPERIMENTAL PROCEDURE

A. WIND TUNNEL TEST SECTION CALIBRATION

Measurement of test section velocity by inserting a pitot-static probe into the test section would create flow disturbances around the airfoil. The wind tunnel test section calibration process established a relationship between the test section dynamic pressure and the measured static pressure differential across the contraction cone. Therefore, a wind tunnel test section velocity can be established by a given static pressure differential.

During the calibration process, a pitot-static probe was inserted into the center of the test section to provide the dynamic pressure (q) measurements. The static pressure differential (Δp) was measured across the static pressure ports on either side of the contraction cone using a micro-manometer. The results are plotted in Figure 4.1.

The tunnel calibration factor (F) is defined by Equation 4.1 [Ref. 13].

$$F = \frac{q}{\Delta P} \tag{4.1}$$

Application of a linear curve fit resulted in a slope, which corresponds to F, of 1.081.

Once F has been determined, test section velocity can be calculated from ΔP using the relationship of Equation 4.2.

$$v = \sqrt{\frac{2\Delta PF}{\rho}} \tag{4.2}$$

Using appropriate conversion factors and a tunnel calibration factor of 1.081, Equation 4.2 reduces to:

$$v = 11.93\sqrt{\frac{\Delta P}{\rho}} \tag{4.3}$$

with ΔP measured in cm of water, ρ in slug/ft^3, and velocity in ft/sec.
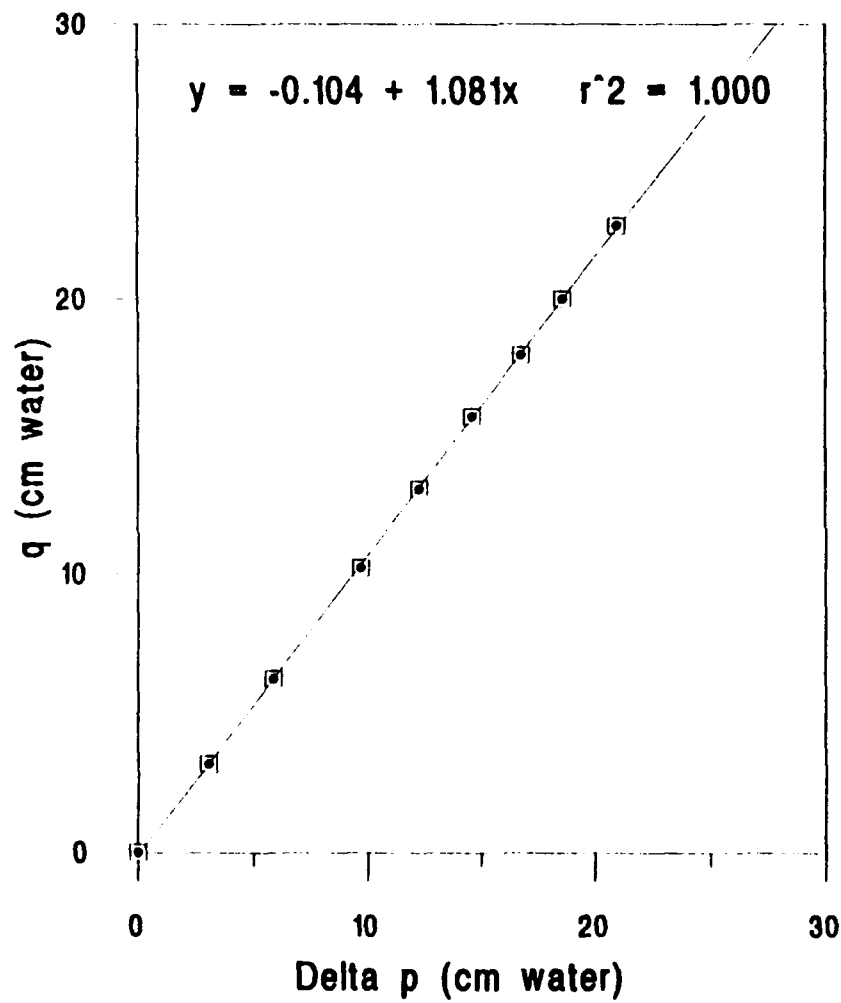
Figure 4.1: Wind Tunnel Test Section Calibration Factor Plot

With test section velocity known, the chord Reynolds number may be calculated using Equation 4.4.

$$R_c = \frac{v\rho c}{\mu} \qquad (4.4)$$

B. PRE-RUN PROCEDURES AND ADJUSTMENTS

The following procedures and adjustments were performed to access the instrument control and readout via PANELS, adjust the wheatstone bridge excitation voltages, zero the amplifier, and zero each amplified wheatstone bridge output voltage. Setup and connections were performed in accordance with Chapter III.

The power switches for the signal conditioner, HP Instruments, and Fluke DMM are located on the front panel of the respective unit. The power for the amplifier is switched on via a junction box at the rear of the rack. Power was applied to these units at least an hour prior to experiments or calibration to stabilize system drift. The amplifier and signal conditioner remained powered constantly during the experimental and calibration periods.

To access the microcomputer control and display of the HP Instruments, <u>PANELS</u> was entered following the C: prompt. Using the cursor, <u>Etc.</u> was selected in the lower right corner and then <u>Enable Outputs</u> on the bottom row. A note appeared and the <u>Enable</u> box, at the right margin illuminated to confirm selection. The cursor was used to roll up the instrument selections, located along the left margin, until <u>Relay Mux .01</u> and <u>DMM</u> appeared. <u>Relay mux .01</u> was selected and then channel <u>8</u>. <u>DMM</u> could then be selected to provide a full screen display, or the voltage can be read along the left margin, below the <u>DMM</u> selection box.

The front panel of the signal conditioner contains two potentiometers and two output jacks for each channel. The Fluke DMM, located below the signal conditioner, was connected across the upper output jacks to measure the excitation voltage, while

31

the lower potentiometer was used to adjust the excitation voltage to 5.00 ± 0.003 Vdc. This procedure was performed for each balance channel.

With Channel 8, the grounded channel, selected on the relay multiplexer, the amplifier was zeroed as follows. The upper portion of the amplifier contains two screws labeled "zero out" and "zero in", and a gain adjust knob. With the gain set to one, the "zero out" screw was adjusted until a voltage reading of 0.0 ± 200 μVdc was obtained. A gain of 1000 was then selected and using the "zero in" screw, the voltage was adjusted to 200 ± 0.5 mVdc. This 200 mVdc offset was selected due to the instability of the amplifier at zero volts.

The model, or calibration bar, and strain gage balance shafts were then set to the angle of attach (AOA) desired during the calibration or experiment run. The 200 mV offset voltage was then set for each balance channel. Using the relay multiplexer, soft panel channel 2 was selected. the upper potentiometer on the signal conditioner front panel was used to adjust the balance channel voltage to 200 ± 0.5 mVdc. This procedure was repeated for each balance channel.

V. RESULTS

A. MAGNITUDE OF AMPLIFIED OUTPUT VOLTAGES

The magnitude of the amplified output voltages at the design load and amplifier gain of 1000 was calculated to be 11.66 Vdc and 0.23 Vdc for the normal and axial directions, respectively. The design loads are 113.0 lbf and 3.0 lbf in the normal and axial directions, respectively. These values result in 1.03 Vdc per 10 lbf normal force and 0.77 lbf per 1 lbf axial force.

The amplified output voltage produced by amplifier A for Channel 2, the normal direction, was 0.28 Vdc per 10 lbf, and 0.06 Vdc per 1 lbf for Channel 3, the axial direction. Amplifier B produced higher amplified output voltages. Again, Channel 2 was used for the normal direction and Channel 3 for the axial direction. Run #1 produced 0.51 Vdc per 10 lbf and 0.008 per 1 lbf in the normal and axial directions, respectively. Run #2 produced 0.56 Vdc per 10 lbf and 0.007 Vdc per 1 lbf in the normal and axial directions, respectively.

The actual amplified output voltages are an order of magnitude lower than predicted in the normal direction and two orders of magnitude lower in the axial direction. The lower-than-anticipated amplified output voltages in conjunction with excessive drift during calibration resulted in unacceptable variations between successive runs. This response is most prevalent during the force applications at 90 degrees angle of attack (AOA). The anticipated amplified output voltages at the relatively small loadings in the axial direction were overshadowed by the fluctuations caused by drift.

B. SYSTEM DRIFT

Amplifier A possessed significant drift both while at the zero value when no force was applied to the calibration bar and while a force was applied during the calibration process. The drift was erratic, making it impossible to predict and apply corrections to the recorded amplified output voltages. The variations ranged from $\pm$ 0.001 Vdc to $\pm$ 0.003 Vdc during a two-minute period. The two-minute period was selected since it was the interval necessary to complete the wind tunnel startup and to perform the measurements. As a result of the drift, prior to each successive force application during the calibration process of amplifier A, all channels were rezeroed to ensure a degree of accuracy of the results. The results of this process are discussed later in this chapter.

The system drift was investigated after installation of amplifier B. Although all four channels did drift slightly while at the zero value, it was significantly less than the drift encountered with amplifier A. The drift experienced while a force was applied was of concern since this drift would alter the recorded amplified output voltages. Appendix E contains the tabular amplified output voltages of system drift during a 15-minute investigation with a 25-lb force applied. A summary of the drift during the 15-minute period of each channel is shown in Table 5.1:

TABLE 5.1: 15-MINUTE SYSTEM DRIFT

Channel 2	- 0.0013 Vdc
Channel 3	+ 0.0008 Vdc
Channel 4	- 0.0020 Vdc
Channel 5	+ 0.0003 Vdc

The system drift recorded during a 5-minute period are as shown in Table 5.2:

TABLE 5.2: 5-MINUTE SYSTEM DRIFT

Channel 2	- 0.00063 Vdc
Channel 3	+ 0.00023 Vdc
Channel 4	- 0.00130 Vdc
Channel 5	+ 0.00001 Vdc

The drift during the 5-minute period is considered to be negligible for Channels 2, 3, and 5. Although the drift for Channel 4 is -0.0013 Vdc, during the first 5-minute interval this drift was shown to decay to 0.00049 Vdc and 0.00021 Vdc for the second and third 5-minute intervals, respectively. Therefore, system drift is not believed to have a significant adverse effect on the recorded amplified output voltages.

C. REPEATABILITY

The major concern during the calibration process was ensuring repeatability. If repeatability can not be achieved during the calibration process, the amplified output voltages can not be converted to forces with any degree of certainty during airfoil testing.

Using amplifier A, the calibration runs were conducted at 0 degrees AOA. During each of these calibration runs, the loading sequence was varied to ensure that there was no dependence on loading sequence. The tabular data of amplified output voltages and calibration curves are contained in Appendix B. The amplified output voltages for these various runs and loading sequences are consistent, providing good repeatability. The largest variation between any two particular runs occurred at 0 degrees AOA with 40-lb. force and was 0.0083 Vdc for Channel 2 and 0.0036 Vdc for Channel 4. A

discontinuity exists between 30 lb and 40 lb loading at 0 degrees AOA. This corresponds to the loading at which the greatest variation between runs exists. This discontinuity will be discussed in detail elsewhere in this chapter.

For the remainder of the 0 degrees AOA and 90 degrees AOA runs, the variation is approximately an order of magnitude less or 0.0001 Vdc between successive runs. As a result, the repeatability displayed using amplifier A was deemed adequate to provide confidence in the measured results during airfoil testing.

The repeatability of amplifier B did not follow the same trend set by amplifier A. The calibration process of amplifier B consisted of two independent runs at both 0 degrees AOA and 90 degrees AOA. During run #1 at 0 degrees AOA, the forces were successively increased in 10 lb increments up to 70 lb, while rezeroing prior to each force application. The odd-numbered forces were applied using the same technique beginning at 65 lb and decreasing in 10 lb increments. Procedure for Run #1 at 90 degrees AOA was identical except for performing in 2 lb increments. Force applications during Run #2 at both 0 degrees AOA and 90 degrees AOA were performed in ascending order beginning and ending with a measurement taken at 0 lb force. Again, to ensure system drift was not altering the amplified output voltages and since actual tunnel measurements were to be performed in this manner, the readings of all channels were rezeroed prior to each force application. The tabular amplified output voltages and calibration curves for Runs #1 and #2 are contained in Appendices C and D, respectively.

A comparison between amplifier B runs #1 and #2 reveals a lack of repeatability between the two runs. At 0 degrees AOA, Channel 2 displayed the largest variation between successive runs. The variation ranged from 0.047 Vdc at 10 lb force to 0.398 Vdc at 50 lb force. The remainder of the variations averaged approximately 0.28 Vdc. At 0 degrees AOA, Channels 3, 4 and 5 displayed variations approximately an order of

magnitude less than that of Channel 2. This variation, however, was large enough to affect repeatability. At 90 degrees AOA, the variation between the two runs is as much as an order of magnitude of the amplified output voltages. All four channels had a high degree of variation at specific force loadings, which ruled out the belief that Channel 2 displays the most significant drift as shown during the runs at 0 degrees AOA. Table 5.3 shows the maximum variation of each channel during the 90 AOA calibration runs.

TABLE 5.3: REPEATABILITY INVESTIGATION

Channel 2	0.0027 Vdc
Channel 3	0.0140 Vdc
Channel 4	0.0081 Vdc
Channel 5	0.0123 Vdc

Although the variations for Channels 2 and 4 are relatively small, their effect on the amplified output voltages is significant due to the small magnitude of signal. This fact is discussed elsewhere in this chapter.

In an attempt to determine the source of the amplified output voltage variation, a constant load was applied in repetition. At 0 degrees AOA with a 30 lb force, the variation between three runs ranged from 0.009 Vdc for Channel 3 to 0.032 Vdc for Channel 2. During the investigation conducted at 90 degrees AOA with a 5 lb force, the variation ranged from 0.00067 dc for Channel 4 to 0.00034 Vdc for Channel 2. Therefore, a repetitive loading is shown to provide repeatability. The plots of the repeatability investigation are contained with Appendix F.

D. AIRFOIL FAILURE

Since the outer airfoil sections are simply cantilever beams extending from the vertical side supports, they are free to flex in a plane perpendicular to the airfoil chord. This bending was a consideration during the iterations of the design phases. The 1.2 inch by 0.7 inch quarter-chord cutout was sized to ensure enough material remained to provide adequate strength in that direction to preclude failure and excessive deflections.

Due to the difficulty of constructing the outer airfoil sections with the quarter-chord cutout, they are comprised of multiple pieces of mahogany which are glued together along chordwise joints. Each of these pieces is approximately 0.75 inches in width.

During the testing phase, one of the outer airfoil sections failed along the chordwise direction. This failure allowed the entire outer airfoil section to contact the strain gage balance shaft which was enclosed within the quarter chord cutout. As a result of this unexpected loading, the strain gage balance shaft deflected to an extent which rotated the insert, contained within the center airfoil section, downward off the longitudinal axis of the airfoil.

The location of the chordwise failure, or crack, of the outer airfoil section does not correspond to an adhesive joint of the airfoil. The crack drifts inward approximately 0.5 inches as it progresses from the leading edge to the trailing edge. There also exists multiple smaller cracks, of approximately 2.0 inches in length, which propagate at the same position of the leading edge.

The opposite outer airfoil section was inspected but no indication of failure nor impending failure was evident. During the wind tunnel run, the alignment of the opposite outer airfoil and center airfoil sections were observed and no discrepancies were noticed. Therefore, this failure is deemed to be an isolated incident caused by a defect in the wood used for construction rather than a design flaw. Although failure

was not anticipated, the design precludes the outer airfoil sections from being sent downstream since the strain gage balance shafts run through the outer airfoil section.

VI. CONCLUSIONS AND RECOMMENDATIONS

A. CONCLUSIONS

The problems encountered during the calibration phase are attributed to faulty amplifiers. These problems included excessive drift of the amplified output voltages both at zero loading and during force applications and possibly are a contributing factor to the lack of repeatability and magnitude of amplified output voltages.

The problems of system drift were overcome using amplifier B. Repeatability, however, was poor with the second amplifier. Although changing to amplifier B did double the amplified output voltages achieved during the 0 degrees AOA calibration runs, the values remained an order of magnitude less than calculated. With these considerations, it is concluded that either both amplifiers A and B are not operating properly or other unresolved factors within the data acquisition system or strain gage balance shafts are creating variations which render the calibration useless.

B. RECOMMENDATIONS

Due to the problems encountered with the data acquisition system believed to have been caused by the amplifiers, it is recommended that the entire system be checked for other possible causes of the errors encountered. The amplifiers should be recalibrated to ensure their proper operation, and replaced if necessary. It is also recommended that periodic maintenance and testing be performed to preclude the untimely setbacks encountered during this investigation. Furthermore, dedicated assistance from a qualified technician, familiar with troubleshooting and normal operations, would have alleviated a significant amount of unproductive time and assumptions.

The airfoil failure is attributed to an irregularity within the wood due to the localized failure. Therefore, the only specific recommendation to prevent further similar failures is to construct the airfoil of a material such as aluminum. Redesign of the outer airfoil section attachment to the vertical side supports may reduce the possibility of airfoil failure.

41

APPENDIX A
Construction Drawings

SEE NOTE 3

18.28

NOT TO SCALE

2.00

THROUGH Ø .52

SEE NOTE 1

8.00

NOTES:
1. REFERENCE DRAWING #3 FOR INSERT CONFIGURATION.
2. WOOD - LAMINATE CONSTRUCTION.
3. THROUGH-HOLE FOR COUNTER SUNK, THREADED ROD.

SCALE: NONE	APPROVED BY:	DRAWN BY: RKJ
DATE: 1 OCT 91		REVISED
2-D AIRFOIL - CENTER SECTION		
NACA 0012		
		DRAWING NUMBER
		1 OF 7
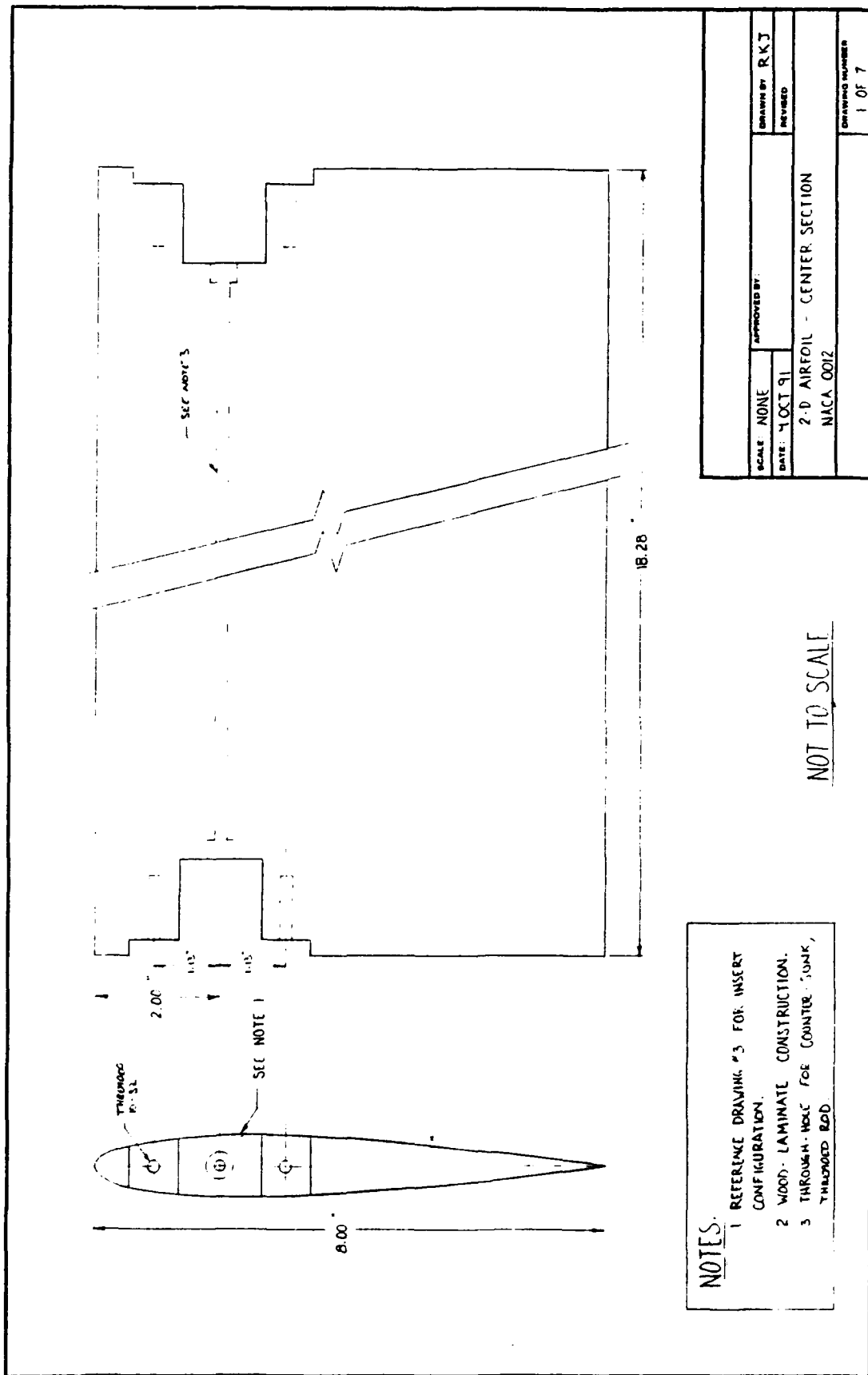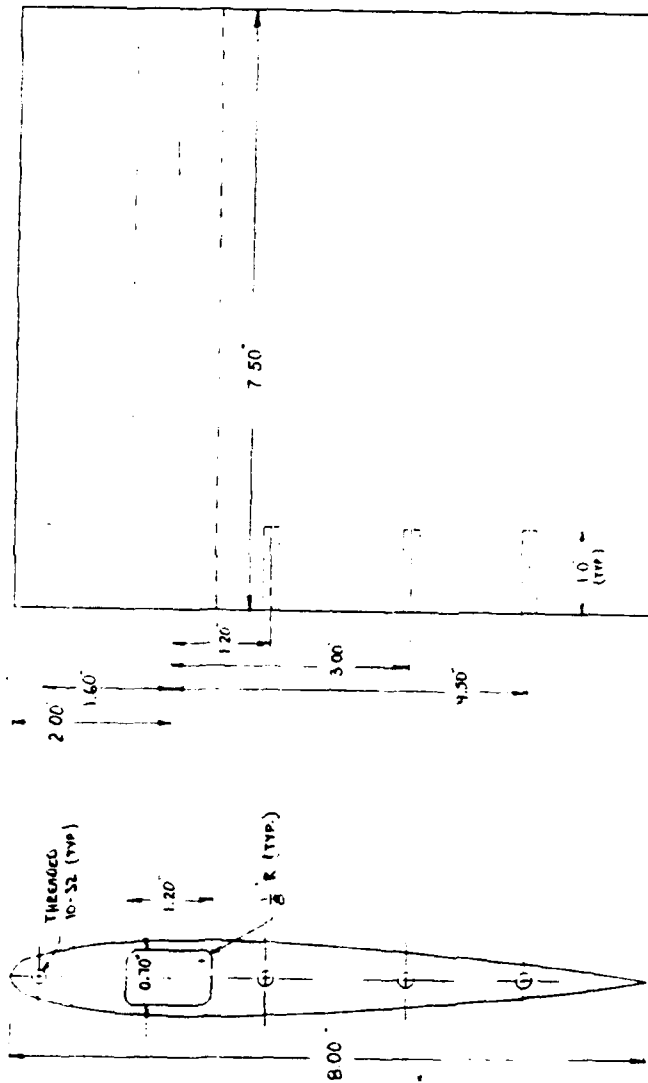
NOT TO SCALE

NOTES
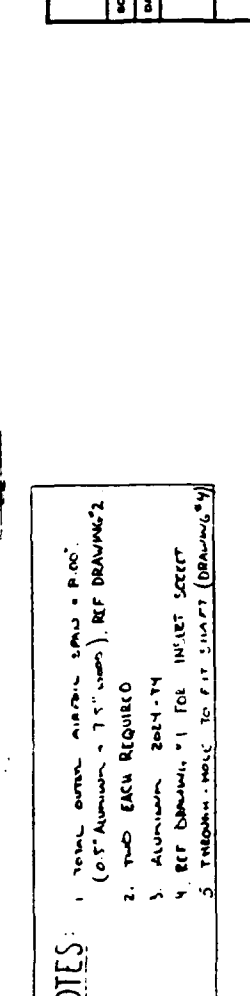
1 REF DRAWING N° 3 FOR END CAP CONFIGURATION

2 TWO REQUIRED

3. WOOD - LAMINATE CONSTRUCTION

THREADED 10-32 (TYP)

1.20

⅛ R (TYP.)

0.70

8.00

7.50

1.20

3.00

4.50

2.00

1.60

1.0 (TYP.)

SCALE: NONE	APPROVED BY:	DRAWN BY: RKJ
DATE: 4 OCT 91		REVISED

2-D AIRFOIL - OUTER SECTION (TYPICAL)
NACA 0012

DRAWING NUMBER: 2 OF 7

NACA 0012 COORDINATES
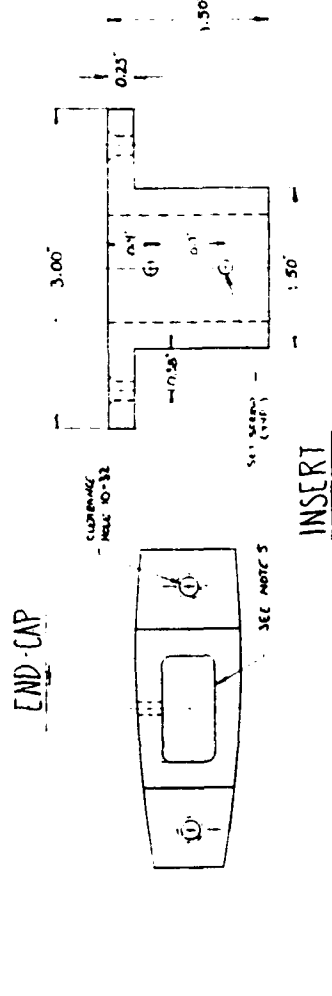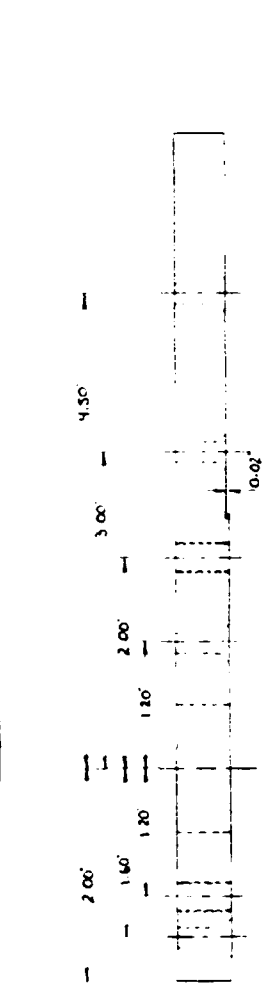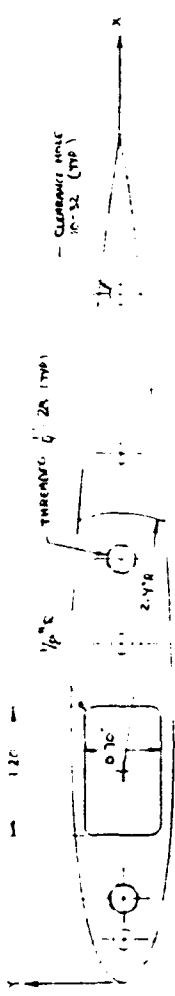
X (mm)	± Y (mm)
0	0
0.1	0.152
0.2	0.209
0.4	0.284
0.6	0.336
0.8	0.375
1.2	0.428
1.6	0.459
2.0	0.475
2.4	0.480
3.2	0.464
4.0	0.424
4.8	0.365
5.6	0.293
6.4	0.210
7.2	0.116
7.6	0.065
8.0	0

END-CAP

INSERT

NOTES:
1. TOTAL OUTER AIRFOIL SPAN = 8.00" (0.5" ALUMINUM + 7.5" WOOD). REF DRAWING #2
2. TWO EACH REQUIRED
3. ALUMINUM 2024-T4
4. REF DRAWING #1 FOR INLET SCREEN
5. THROUGH-HOLE TO FIT SHAFT (DRAWING #4)

2 REQ'D

SEC A-A

SEC B-B

SEC C-C

10.00"

0.50

0.75

2.285"

0.75

1.05"

1.00

0.25

0.50

0.50

0.40

0.25

0.50

1.00"

0.5"

1/16 R (TYP)

SCALE: 1" : 0.5"	APPROVED BY:
DATE: 24 OCT 91	DRAWN BY: RKJ
	REVISED
2-D AIRFOIL LOAD MEASURING SHAFT (TYP)	DRAWING NUMBER: 4 OF 7

46
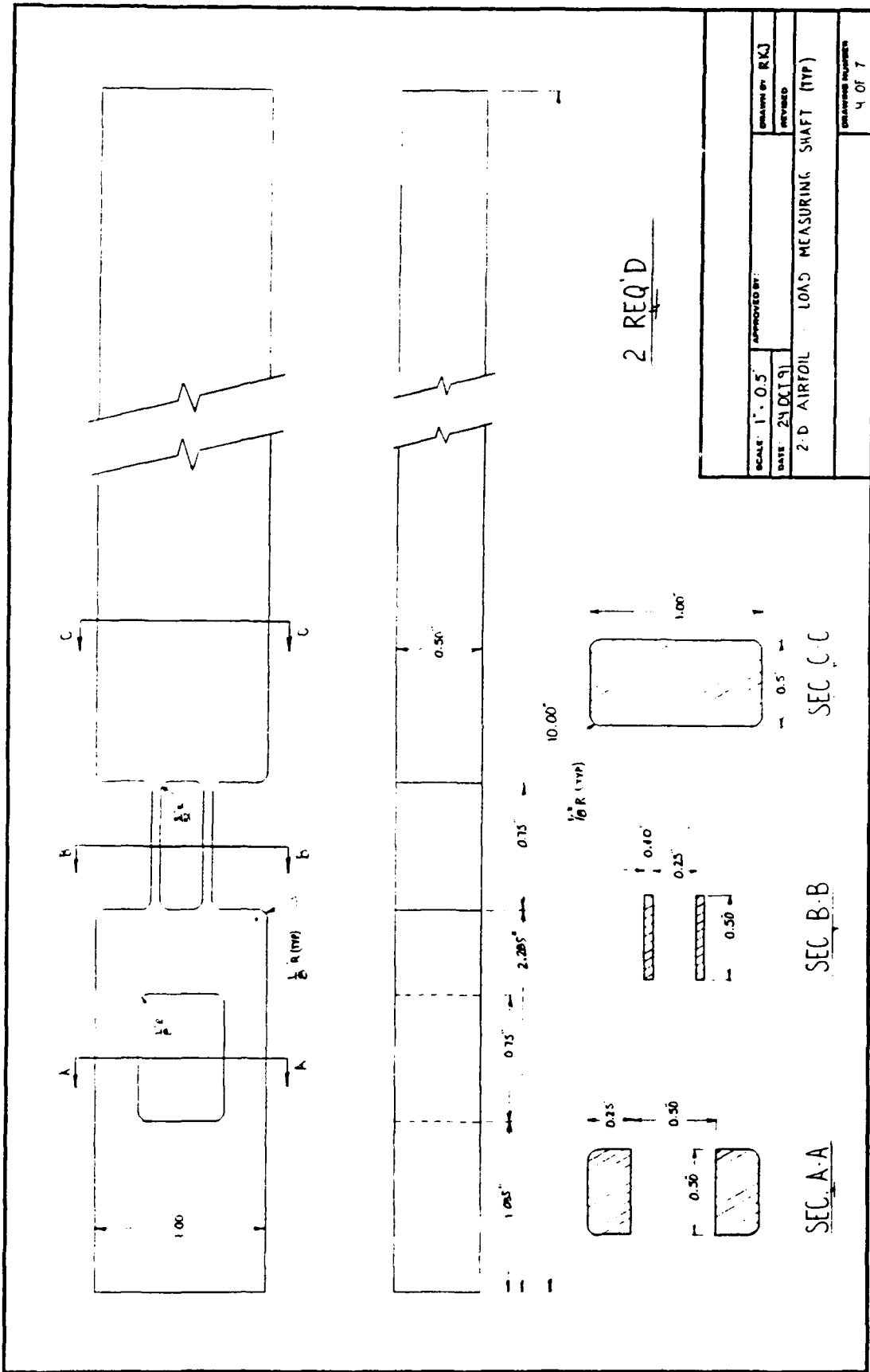
NOTE

CUTOUT TO BE SIZED FOR 1.00 × 0.50"
SHAFT REF DRAWING N° 4

SEE ABOVE NOTE

SEE SCREW (TYP)

-THREADED 5/16 - 24

18.28

9.14"

1.00 (TYP)
.20
.64
.07
1.50 TYP

1.0"
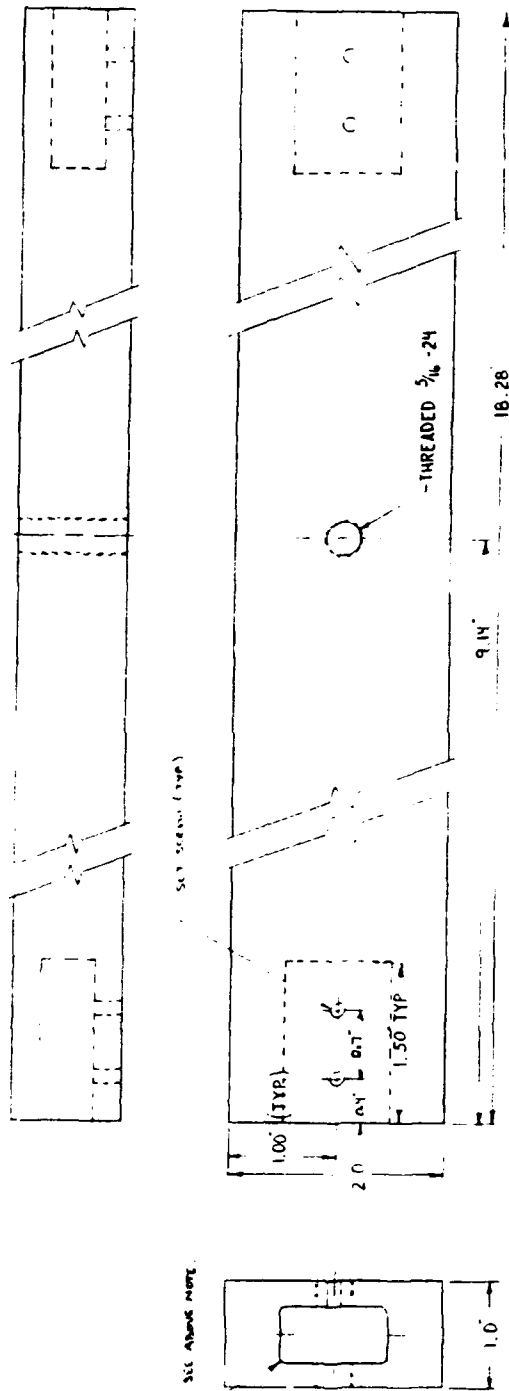
NOTE

CAL BAR TO BE MACHINED FROM ALUMINUM 2024-T4,
OR ALUMINUM WITH EQUIVALENT OR GREATER
YIELD STRENGTH (E - 10 · 10⁶ psi)

48

.5

18.28

34.37

.045 GAP

8.00
(TYP)

APPENDIX B
Amplifier A Plots

CALIBRATION CURVES AT 0 AOA
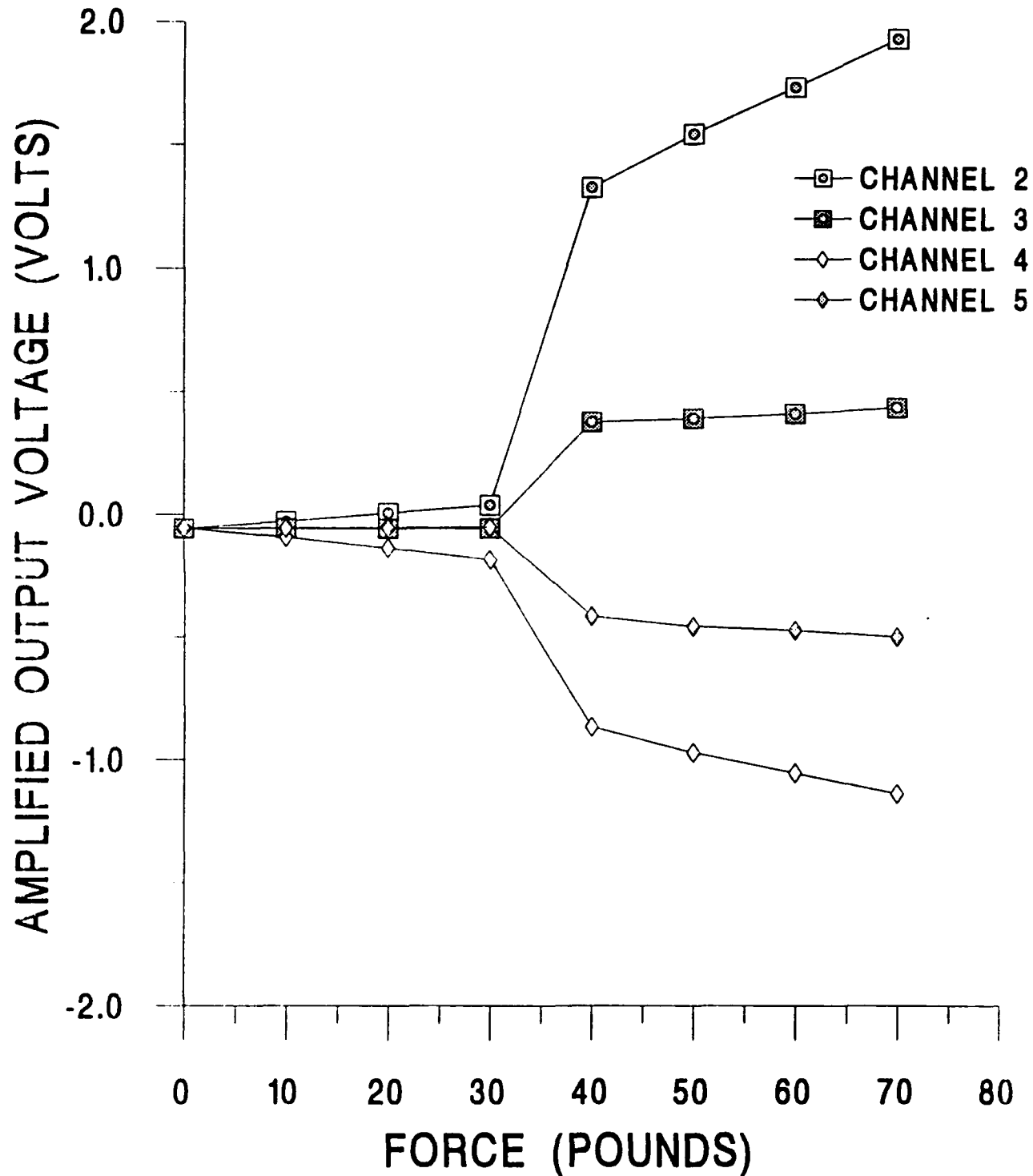
CALIBRATION CURVES AT 90 AOA
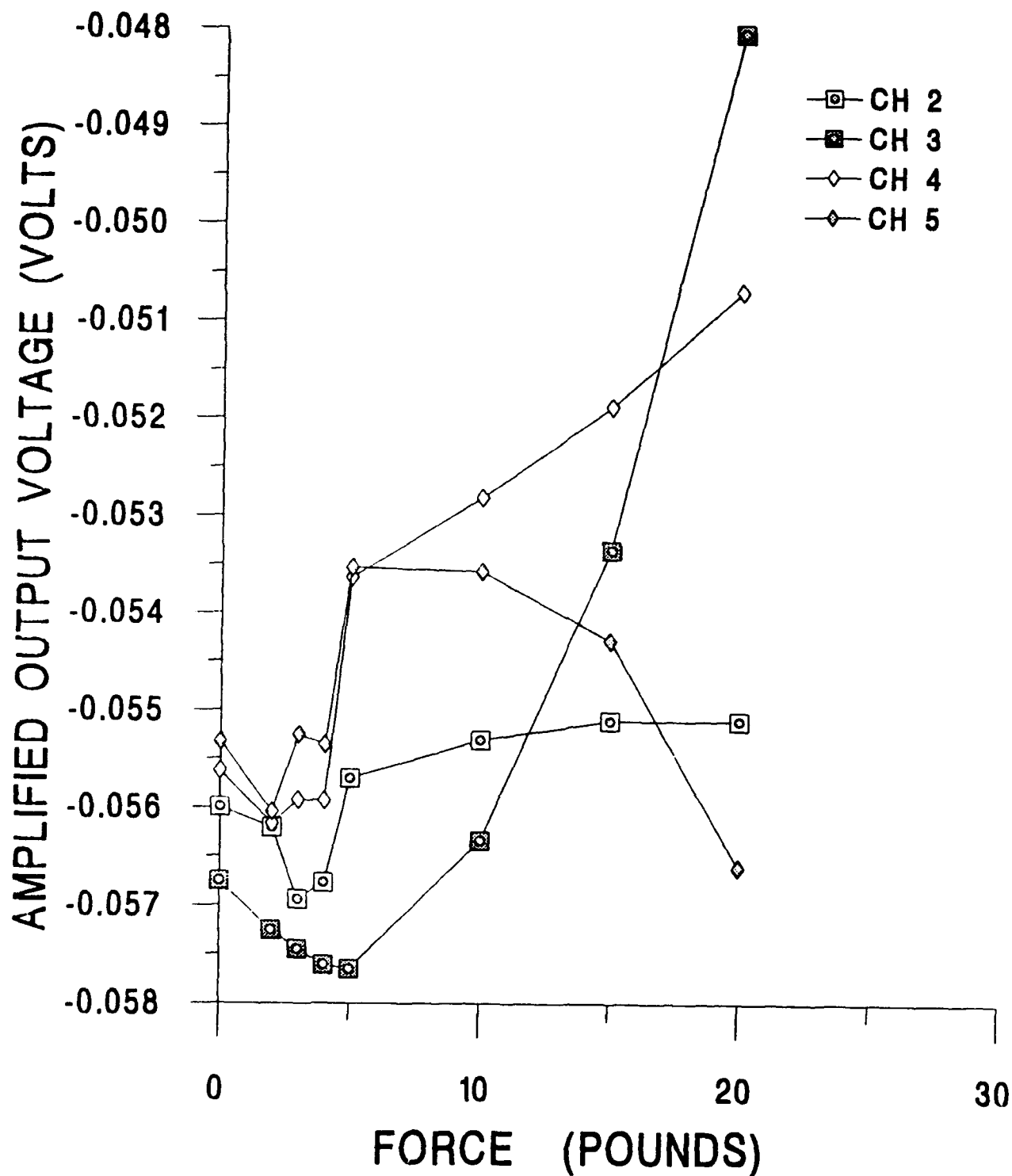
APPENDIX C
Amplifier B Plots - Run # 1

CALIBRATION CURVES AT 0 AOA RUN #1

54

CALIBRATION CURVES AT 90 AOA RUN #1

Figure plotting AMPLIFIED OUTPUT VOLTAGES (VOLTS) versus FORCE (POUNDS) for:
- CHANNEL 2
- CHANNEL 3
- CHANNEL 4
- CHANNEL 5
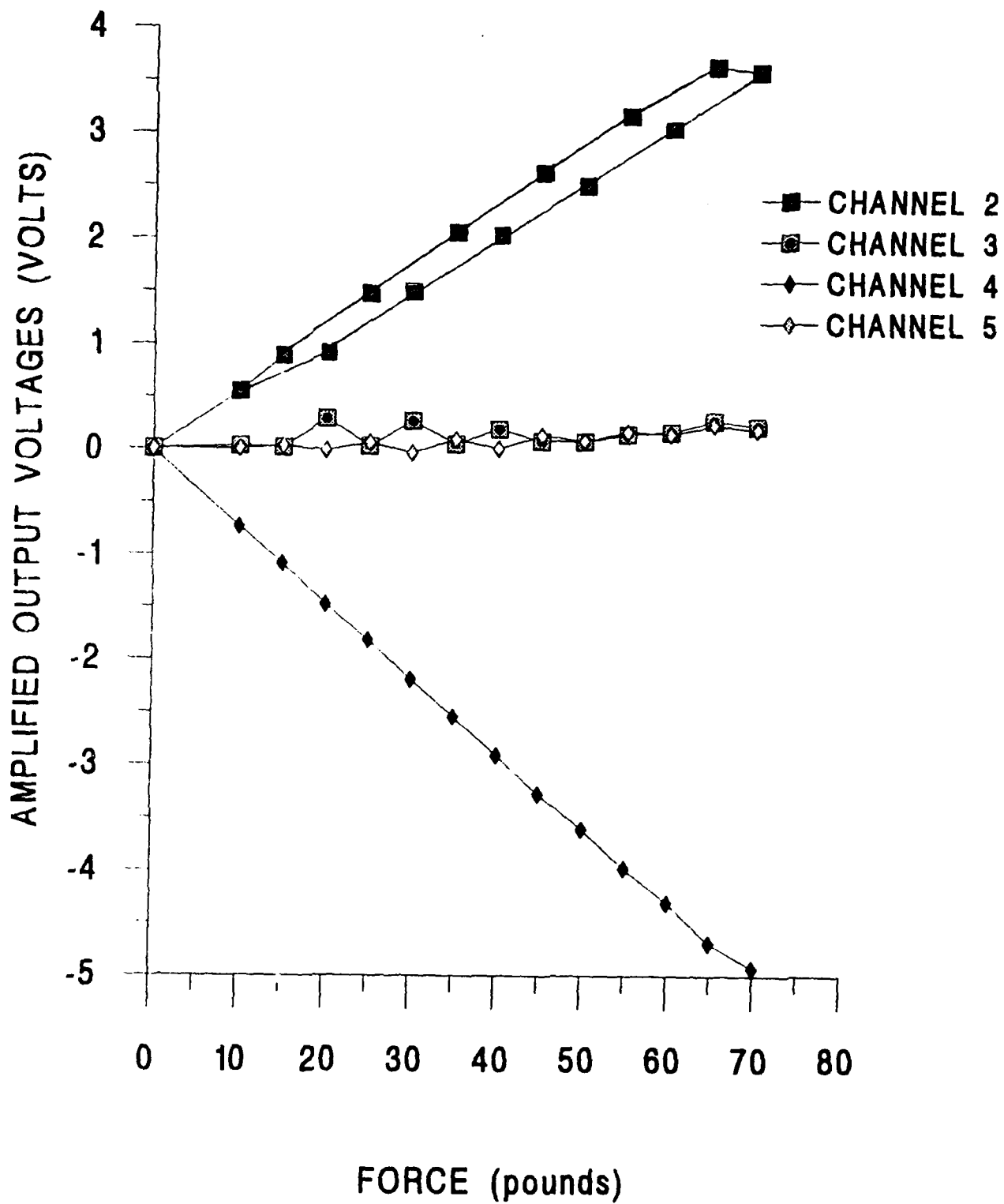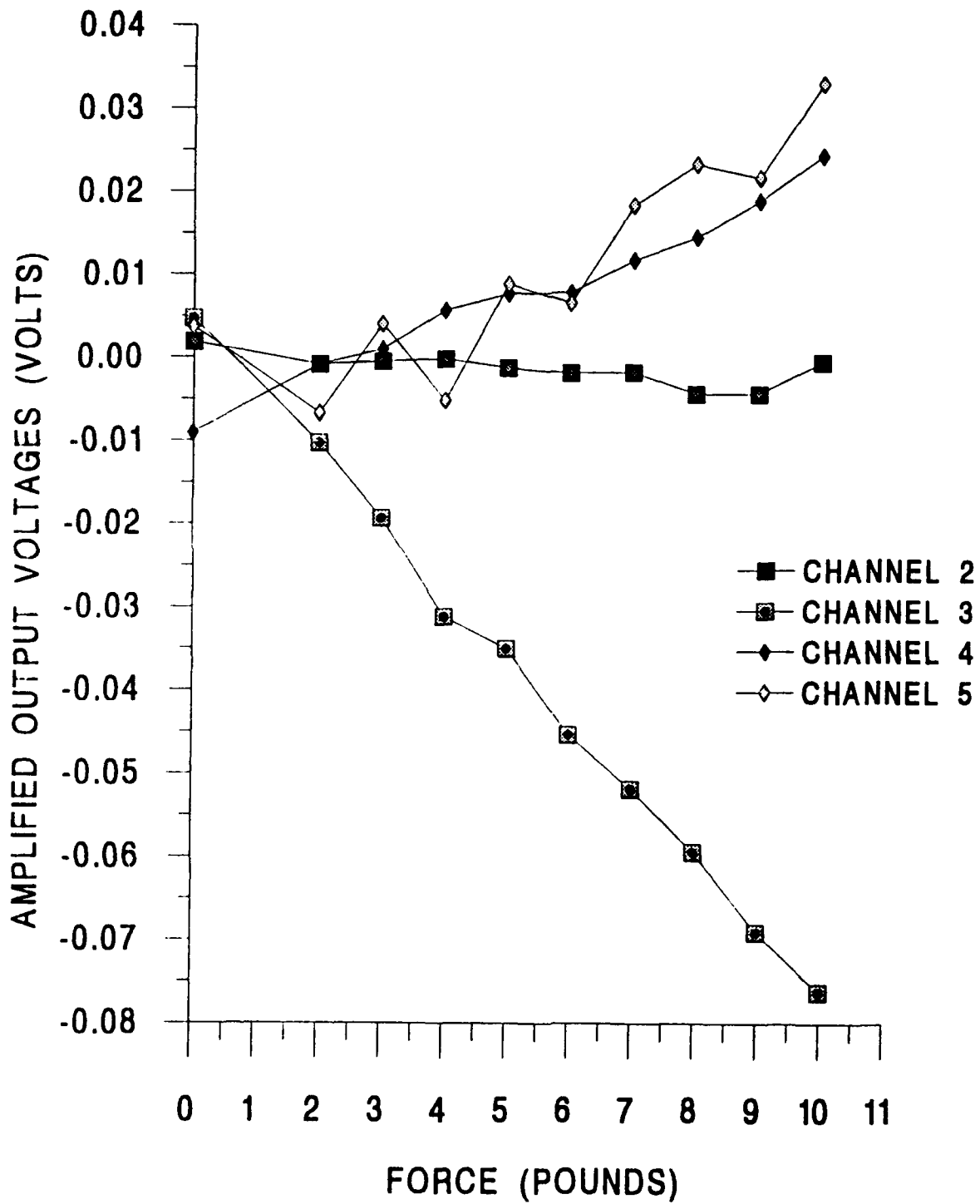
APPENDIX D
Amplifier B Plots - Run # 2

CALIBRATION CURVES AT 0 AOA
RUN #2
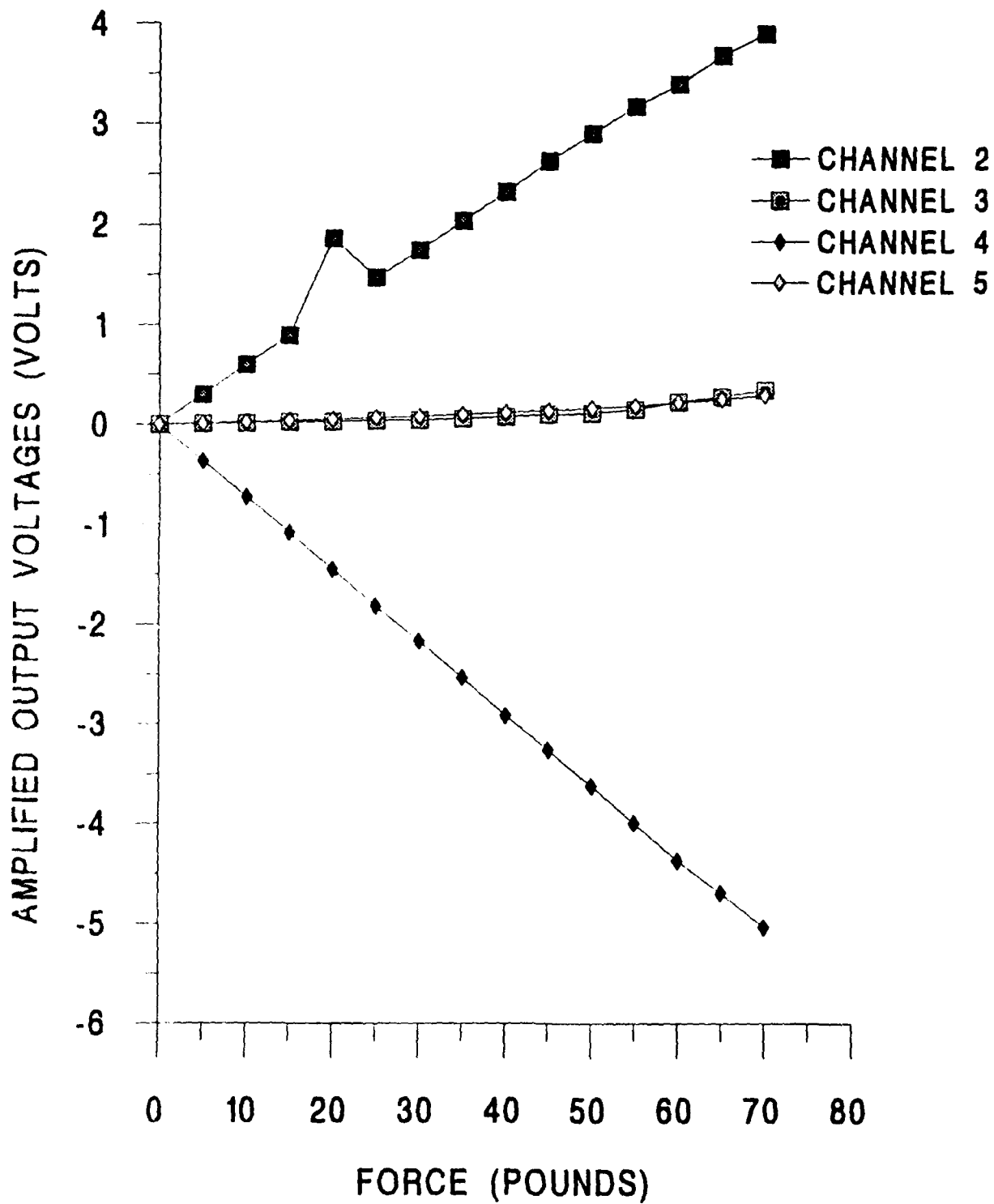
CALIBRATION CURVES AT 90 AOA RUN #2
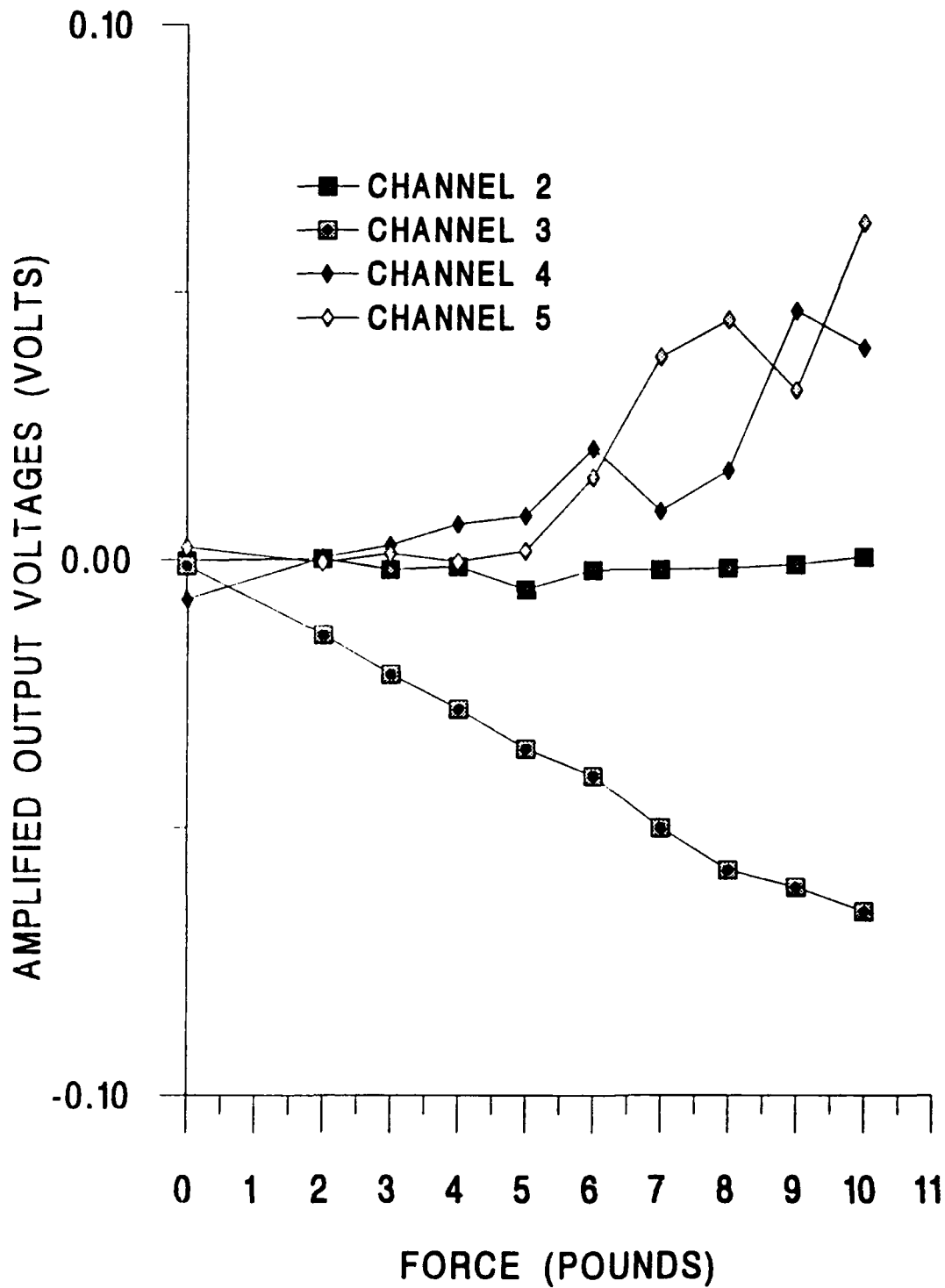
APPENDIX E
System Drift Investigation - Amplifier B

SYSTEM DRIFT T+00
0 AOA / 25 lbs. FORCE

```
IN VOLTS        CH2            CH3           CH4            CH5
********        ***            ***           ***            ***
             %+1.457200    +.035240     %-1.813700     +.065290
             %+1.456900    +.035480     %-1.814000     +.065630
             %+1.457000    +.035220     %-1.812900     +.064790
             %+1.457500    +.034600     %-1.813200     +.064770
             %+1.457300    +.035030     %-1.813700     +.065550
             %+1.456900    +.035740     %-1.813400     +.065570
             %+1.457100    +.035460     %-1.813400     +.065400
             %+1.456800    +.035400     %-1.813500     +.065390
             %+1.456800    +.035270     %-1.813400     +.065310
             %+1.456700    +.035420     %-1.813500     +.065580
READINGS DROP        3            2             2              3
- - - - - - - - - - - - - - - - - - - - - - - - - - - - - - -
MEAN VALUE %+1.456957    +.035315     %-1.813475     +.065441
```

SYSTEM DRIFT T+05
0 AOA / 25 lbs. FORCE

IN VOLTS	CH2	CH3	CH4	CH5
********	***	***	***	***
	%+1.456300	+.035350	%-1.812500	+.065340
	%+1.456000	+.035440	%-1.812700	+.065170
	%+1.456400	+.035530	%-1.812100	+.065450
	%+1.456300	+.035580	%-1.812200	+.065340
	%+1.456400	+.035590	%-1.812100	+.065490
	%+1.456300	+.035540	%-1.812200	+.065470
	%+1.456200	+.035740	%-1.812100	+.064910
	%+1.456000	+.035480	%-1.812300	+.065470
	%+1.456500	+.035760	%-1.812100	+.065500
	%+1.456400	+.035800	%-1.812200	+.065530
READINGS DROP	3	5	2	2
- -
MEAN VALUE	%+1.456329	+.035544	%-1.812163	+.065449

SYSTEM DRIFT T+10
0 AOA / 25 lbs. FORCE

IN VOLTS	CH2	CH3	CH4	CH5
********	***	***	***	***
	%+1.455900	+.035820	%-1.811600	+.065360
	%+1.455600	+.035550	%-1.811600	+.065500
	%+1.455700	+.035780	%-1.811800	+.065530
	%+1.455700	+.035640	%-1.811600	+.065560
	%+1.455800	+.035810	%-1.811600	+.065570
	%+1.455900	+.035720	%-1.811700	+.065760
	%+1.456000	+.035930	%-1.811800	+.065450
	%+1.455700	+.035800	%-1.811700	+.065560
	%+1.455700	+.035520	%-1.810800	+.064360
	%+1.456600	+.034890	%-1.810600	+.064530
READINGS DROP	1	2	2	2
MEAN VALUE	%+1.455778	+.035705	%-1.811675	+.065536

SYSTEM DRIFT T+15
0 AOA / 25 lbs. FORCE

IN VOLTS	CH2	CH3	CH4	CH5
********	***	***	***	***
	%+1.455800	+.036120	%-1.811400	+.065860
	%+1.455600	+.036070	%-1.811500	+.065790
	%+1.455600	+.036040	%-1.811500	+.065840
	%+1.455700	+.036050	%-1.811400	+.065740
	%+1.455600	+.036010	%-1.811800	+.065750
	%+1.455400	+.036030	%-1.811400	+.065830
	%+1.455600	+.036120	%-1.811500	+.065890
	%+1.455700	+.035970	%-1.811500	+.065770
	%+1.455500	+.036260	%-1.811500	+.065770
	%+1.455600	+.036030	%-1.811500	+.065670
READINGS DROP	3	2	1	3
- - - - - - - -	- - - - -	- - - - -	- - - - -	- - - - -
MEAN VALUE	%+1.455629	+.036059	%-1.811467	+.065784

APPENDIX F
Repeatability Plots - Amplifier B

0 AOA / 30 lb. REPEATABILITY

Figure showing amplified output voltages (volts) versus trial for four channels.

Legend:
- ■ CHANNEL 2
- ▣ CHANNEL 3
- ◆ CHANNEL 4
- ◇ CHANNEL 5

Y-axis: AMPLIFIED OUTPUT VOLTAGES (VOLTS)

X-axis: TRIAL
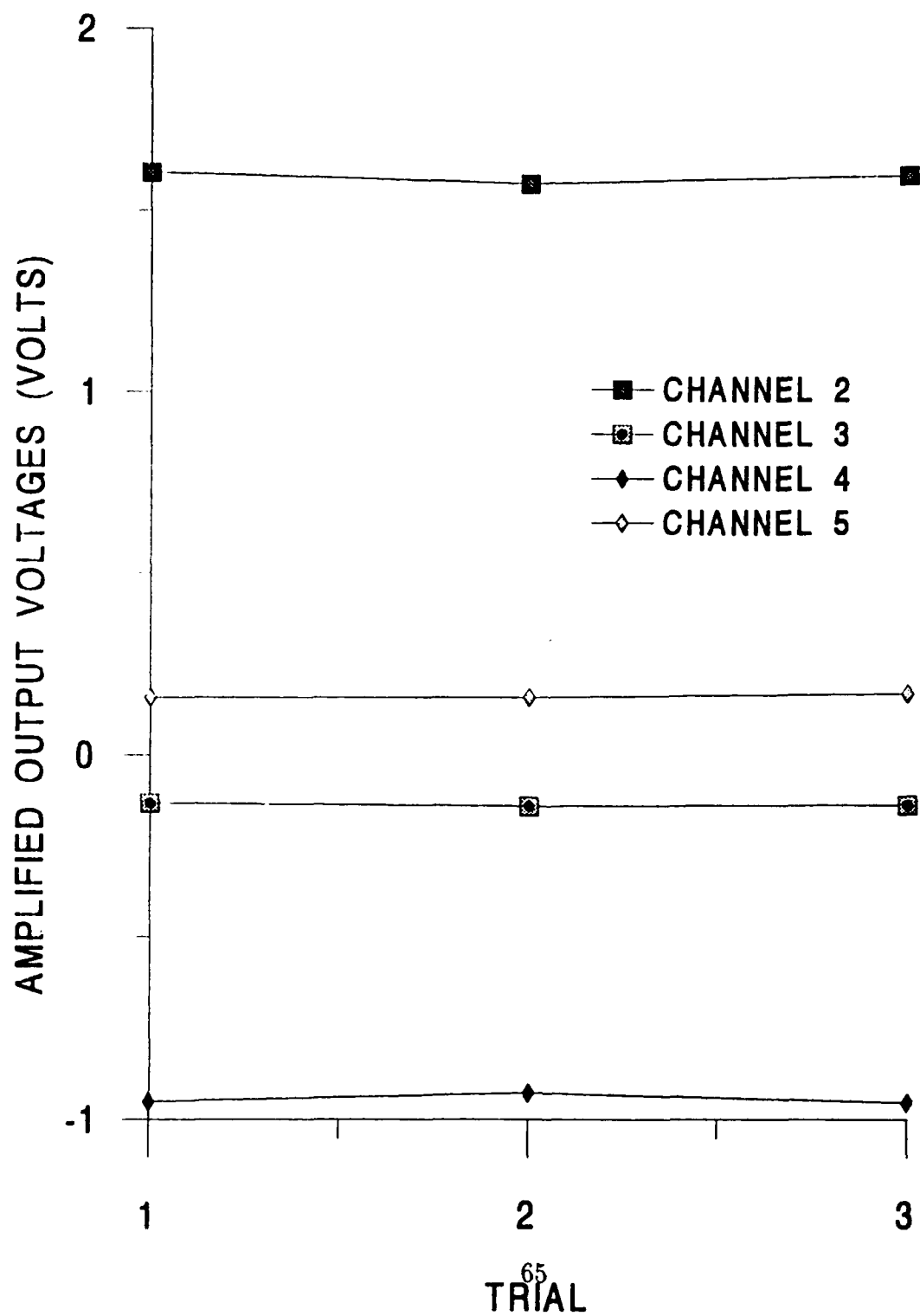
90 AOA / 5 lb. REPEATABILITY
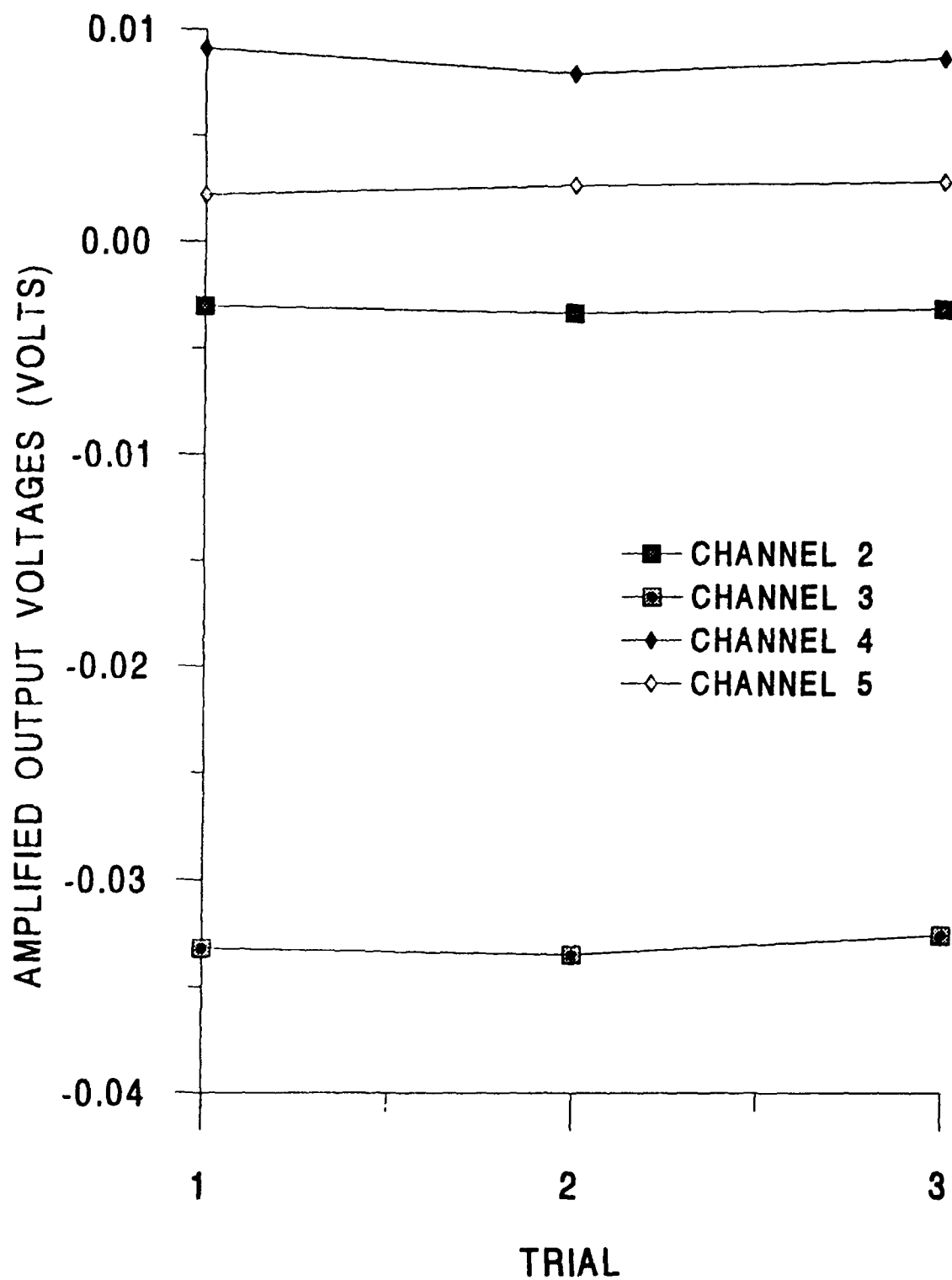
LIST OF REFERENCES

1. Tanner, J. C., *Development of a Flight Test Methodology For A U.S. Navy Half-Scale Unmanned Air Vehicle*, Master's Thesis, Naval Postgraduate School, Monterey, California, March 1989.

2. Treaster, A. L., Gurney, G. B., and Jacobs, P. P., Jr., "Sidewall Boundary-Layer Corrections in Subsonic, Two-dimensional airfoil/Hydrofoil Testing," *Jounral of Aircraft*, V. 22, pp. 229-235, March 1985.

3. AGARDograph No. 288, *Low Reynolds Number Vehicles*, by T. J. Mueller, Pp. 12-15, 42-46.

4. AIAA Paper 88-11190, *Low Reynolds Number Wind Tunnel Measurements*, by T. J. Mueller and others, pp. 14.1-14.18, 1988.

5. AGARD Report 292, *A Background to the Problems of Wind-Tunnel Interference*, by E. W. E. Rogers, March 1959.

6. AGARDograph No. 281, *Two-Dimensional Wind Tunnel Wall Interference*, by M. Mokey, Y. Y. Chan and D. J. Jones. pp. 4-5, 36-38, 159-160.

7. AGARD Report 298, *Notes on Half-Model Testing in Wind Tunnels*, by J. A. van der Bliek, March 1959.

8. Naval Sea Systems Command Technical Memorandun 80-44, *A Method of Correcting For The Effects Of The Sidewall Boundary Layer in Two-Dimensional airfoil Testing*, by P. P. Jacobs, Jr., 31 March 1980.

9. Gorlin, S. M. and Slezinger, I. I., *Wind Tunnels and Their Instrumentation*, pp. 394-407, 530-531, 546-547, Israel Program for Scientific Translations, 1966.

10. AIAA Paper 87-2350. *End Plate Gap Effects on a Half Wing Model at Low Reynolds Numbers*, by S. Kuppa and J. F. Marchman, III, pp. 186-195, 1987.

11. Marchman, J. F., "Aerodynamic Testing at Low Reynolds Numbers," *Journal of Aircraft*, V. 24, pp. 107-114, February 1987.

12. Perry, M. L., *The Effects of Leading and Trailing Edge Deflections on the Performance of a Wortmann FX63-137 Airfoil at Low Reynolds Numbers*, Master's Thesis, University of Notre Dame, Notre Dame, Indiana, December 1985.

13. Department of Aeronautics and Astronautics, *Laboratory Manual for Low-Speed Wind Tunnel Testing*, Naval Postgraduate School, Monterey, California, August 1989.

14. Anderson, J. D., Jr., *Introduction to Flight*, 3rd ed., McGraw-Hill, Inc., 1989.

15. Oberg, E., Jones, F. D., and Horton, H. L., *Machinery's Handbook*, 20th ed., Industrial Press, Inc., 1975.

16. Measurements Group, Inc., Micro-Measurements Division, Instruction Bulletin B-129-7, *Surface Preparation For Strain Gage Bonding.*

17. Measurements Group, Inc., Micro-Measurements Division Instruction Bulletin B-127-12, *Strain Gage Installations with M-Bond 200 Adhesive.*

18. Measurements Group, Inc., Micro-Measurements Division, Tech Tip TT-603, *The Proper Use of Bondable Terminals in Strain Gage Applications.*

19. Measurements Group, Inc., Micro-Measurements Division, Catalog 500, *Part A - Strain Gage Listings and Part B Strain Gage Technical Data.*

20. Beer, F. P. and Johnston, E. R., Jr., *Mechanics of Materials*, pp. 153-158, McGraw-Hill, Inc., 1981.

21. Department of Aeronautics and Astronautics, *AE 2801 Laboratory Manual*, Naval Postgraduate School, Monterey, California, January 1990.

INITIAL DISTRIBUTION LIST

No. of Copies

1. Defense Technical Information Center   2
    Cameron Station
    Alexandria, VA 22304-6145

2. Library, Code 52   2
    Naval Postgraduate School
    Monterey, CA 93943-5002

3. Chairman   1
    Department of Aeronautics and Astronautics, Code AA
    Naval Postgraduate School
    Monterey, CA 93943-5002

4. Professor R. M. Howard   2
    Department of Aeronautics and Astronautics, Code AA/Ho
    Naval Postgraduate School
    Monterey, CA 93943-5002

5. Rick J. Foch   1
    Naval Research Lab, Code 5712
    4555 Overlook Avenue S.W.
    Washington, D.C. 20375

6. Lt. Richard Kirk Joyce   1
    NAVCOM Unit Cutler
    P.O. Box 35
    East Machias, ME 04630-1000